Accepted paper

N. Ben Sedrine, J. Rodrigues, D. Nd. Faye, A. J. Neves, E. Alves, M. Bockowski, V. Hoffmann, M. Weyers, K. Lorenz,, M. R. Correia, and T. Monteiro.

Eu-Doped AlGaN/GaN Superlattice-Based Diode Structure for Red Lighting: Excitation Mechanisms and Active Sites. ACS Appl. Nano Mater. 2018, 1, 3845−3858.

10.1021/acsanm.8b00612

ACS APPLIED NANO MATERIALS

Article

www.acsanm.org

Eu-Doped AlGaN/GaN Superlattice-Based Diode Structure for Red Lighting: Excitation Mechanisms and Active Sites

N. Ben Sedrine,*[,†] J. Rodrigues,[†] D. Nd. Faye,[‡] A. J. Neves,[†] E. Alves,[‡] M. Bockowski,[§] V. Hoffmann,[∥] M. Weyers,[∥] K. Lorenz,[‡,⊥] M. R. Correia,[†] and T. Monteiro[†]

[†]Departamento de Física & I3N, Universidade de Aveiro, Campus Universitário de Santiago, 3810-193 Aveiro, Portugal

[‡]IPFN, Instituto Superior Técnico, , Campus Tecnológico e Nuclear, Estrada Nacional 10, P-2695-066 Bobadela LRS, Portugal

[§]Institute of High Pressure Physics, Polish Academy of Sciences, 01-142 Warsaw, Poland

[∥]Ferdinand-Braun-Institut, Leibniz-Institut für Höchstfrequenztechnik, Gustav-Kirchhoff-Straße 4, 12489 Berlin, Germany

[⊥]Instituto de Engenharia de Sistemas de Computadores—Microsystems and Nanotechnology (INESC-MN), Rua Alves Redol, 1000-029 Lisboa, Portugal

Supporting Information

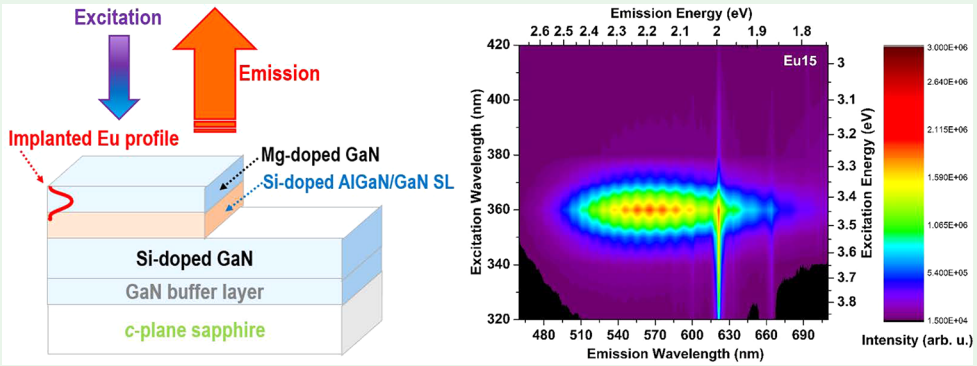

ABSTRACT: In this work, we have established the effects of postgrowth annealing and Eu implantation, followed by annealing on an AlGaN/GaN superlattice-based diode structure, containing Mg-doped GaN top p-cap layers. The study is based on the combined information from different optical techniques, such as Raman, photoluminescence, and photoluminescence excitation. We have shown that the diode structure exhibits a stable crystalline quality even after annealing under high temperature and high pressure (HTHP) conditions (1400 °C in 1 GPa N_2). Furthermore, we have demonstrated that the implanted Eu ions reached the first quantum wells of the diode structure and that the postimplantation thermal annealing partly removed the implantation defects, recovering some of the as-grown luminescence and optically activating the Eu^{3+} in the diode structure. An in-depth study of the Eu^{3+} population mechanisms was realized through room temperature photoluminescence excitation. A model was built based on the different excitation bands originated from the materials present in the diode structure, demonstrating that an energy transfer between the AlGaN/GaN superlattice excitons and the Eu^{3+} ions occurs, therefore enlarging the excitation pathways for the ion's red luminescence. In addition, Eu^{3+} luminescence was observed not only with above but also with below GaN bandgap excitation. The temperature dependent study of the $^5D_J \rightarrow {}^7F_J$ transitions allowed to tentatively provide the Eu^{3+} intraionic assignments of the diode structure. We have demonstrated that at least three nonequivalent active sites are created by the Eu implantation in the diode structure: Eu1, Eu2, and Eu−Mg defect in both configurations Eu0 and Eu1(Mg).

KEYWORDS: *high-temperature and high-pressure annealing, europium, implantation, diode structure, Raman spectroscopy, PL, PLE*

The incorporation of rare earth (RE) atoms into solid hosts, especially wide bandgap III−N semiconductors, have received increasing attention in the last decades due to the potential applications of RE-doped materials in optoelectronic semiconductor devices, such as light emitting diodes (LEDs), solid-state lasers and color displays.[1] The wide variety of growth and doping methods employed over the years, including in situ doping during growth (by molecular beam epitaxy (MBE) or metal−organic chemical vapor deposition (MOCVD)) and ion implantation have reached a considerable progress.[2,3] Besides, in III−N systems, the blue and green light could be obtained based on InGaN bandgap engineering, while the red emitters are still under research and development. A possible solution for achieving the red emission is the use of europium (Eu)

Received: April 13, 2018
Accepted: July 17, 2018
Published: July 17, 2018

DOI: 10.1021/acsanm.8b00612
ACS Appl. Nano Mater. XXXX, XXX, XXX−XXX

doping into III−N hosts thanks to the luminescence determined only by Eu^{3+} intra-4f^6 transitions. Nishikawa et al.[4,5] have realized red-emitting LED by using in situ Eu-doped GaN active layer. For nominally undoped GaN samples implanted with Eu, thermal annealing at high temperatures was established to lead to the formation of two dominant optical centers denoted as Eu1 and Eu2,[6,7] where the first center (Eu1) involves Eu_{Ga} associated with intrinsic lattice defects,[8] while the second (Eu2) is a substitutional Eu impurity (Eu_{Ga}). For such samples, postimplantation annealing at temperatures in the range of 1000−1450 °C in high N_2 pressure, a predominance of Eu2 optical center was demonstrated.[8] Alternatively, other authors have attributed the Eu1 and Eu2 centers to complex defects involving the Eu^{3+} ion in a substitutional cation position with next-neighbors being N and Ga vacancies, respectively.[9,10]

Furthermore, codoping GaN:RE with additional impurities was demonstrated to be a powerful technique to control Eu centers and improve the luminescence. For instance, magnesium (Mg) doping enhances the RE luminescence efficiency in GaN[11,12] because it is expected to modify local structures around the RE ions. In this context, O'Donnell et al.[13,14] attributed the observed photoenhancement, temperature hysteresis, and photobleaching to conformational modifications because the change of the charge state of the (Eu−Mg)-related defects in p-type GaN. The same strategy of Mg and Eu codoping in GaN was used to probe the lattice location of Mg in GaN (Mg):Eu[15,16] by hysteresis photochromic switching between two configurations (Eu0 and Eu1(Mg)) of the same Eu−Mg defect: Eu_{Ga} in close association with Mg_{Ga} bonded to a common N atom.[16] Wakahara et al.[1] also investigated the effect of Mg codoping on the luminescence properties of Eu-doped GaN epitaxial films for different Mg concentrations, and demonstrated that the optimal doping of Mg in GaN:Eu led to the selective activation of site-A (~620.3 nm), with respect to site-B (~622.3 nm), resulting in an enhanced Eu^{3+} luminescence. As a result, the authors fabricated a LED with p-GaN/GaN:(Eu, Mg) active layer/n-GaN structure using optimal Mg codoping conditions (~10^{18} cm^{-3}) and obtained bright red emission under forward bias condition. On the other hand, unlike nitride bulk or layers, it was demonstrated that the intensity of the emission is enhanced when the RE ions are implanted in quantum structures, such as quantum wells (QWs) and superlattices (SLs),[17] as obtained in Eu[18,19] and erbium (Er)[20] implanted in AlGaN/GaN SLs. Furthermore, according to Favennec's principle, wider bandgap semiconductors show weaker thermal quenching, thus favoring the III-nitrides among other semiconductors.[21] Indeed, it was proven that thermal quenching of photoluminescence (PL) intensity became very small with the increase of Al content in AlGaN epitaxial layers.[22] O'Donnell[23] have demonstrated this principle by showing that the $T_{1/2}$ value (corresponding to the temperature at which the intensity of the luminescence is one-half of its maximum low-temperature) is as high as 400 K for GaN, but this value strongly depends on the RE related center in the III−N host. Recently, a synergy effect between the increase of III−N bandgap and the codoping was explored by Kanemoto et al.[24] for Mg codoped AlGaN:Eu epitaxial films. It was found that Mg codoping in AlGaN:Eu contributes to increase the PL integrated intensity and to improve the PL efficiency. Mishra et al.[25] also reported a strong enhancement of the Eu^{3+} luminescence by simultaneously codoping with silicon (Si) and Mg in Eu-implanted GaN samples. In addition to the intensity enhancement, Lee et al.[26] showed that Mg codoping into GaN:Eu produced novel Eu−Mg luminescence centers, while the addition of silicon removed such centers and enhanced an additional one.

In this work, we deeply investigate Eu implantation followed by high-temperature high-pressure (HTHP) annealing in an AlGaN/GaN superlattice- based diode structure, as an alternative approach to in situ doping to provide additional solutions for the red emission issue in the III−N systems. To do so, optical techniques were used to explore: (i) the effects of postgrowth HTHP annealing of the as-grown diode structure and (ii) the effects of Eu implantation followed by HTHP annealing. The Eu^{3+} population mechanisms were established and the Eu^{3+} emission lines and their temperature dependence were analyzed in detail.

METHODS

The diode structure (Figure S1) was grown by MOCVD on a thick GaN buffer layer on sapphire substrate. The n−p junction was formed by Si-doped GaN (n-type, free carrier concentration ~2.5×10^{18} cm^{-3}) and Mg-doped GaN (p-type, free carrier concentration ~5×10^{17} cm^{-3}), with nominal thicknesses of ~2300 nm and ~100 nm, respectively. A 100-period n-type AlGaN/GaN short period superlattice (SL), with nominal thickness of ~2.5 nm for $Al_xGa_{1-x}N$ (nominal AlN content of ~0.14) and GaN layers, both Si-doped (Si concentration ~1×10^{18} cm^{-3}), was inserted on top of the n-GaN layer to provide carrier confinement. In addition, the high number of interfaces prevents Mg diffusion during temperature steps and therefore the shift of the p-doped region with respect to the Eu implanted region. X-ray diffraction (XRD) measurements and simulations show a good agreement of layer thicknesses and composition with the nominal structure, with well-defined SL peaks revealing a good interface quality of the SL.[27] Ion implantation was carried out using 300 keV Eu ions at room temperature (RT), along the surface normal, and with two different fluences (1×10^{14} and 1×10^{15} Eu·cm^{-2}). Such channeled implantation conditions were found to reduce the implantation defect density and increase the ion range.[28] The Eu-profile simulation, using the SRIM code and assuming no channeling effects, suggests that the maximum ion penetration depth is ~120 nm, indicating that only few ions actually reach the p−n junction for such implantation conditions.[27] Postimplantation HTHP annealing was then performed for 30 min at 1400 °C in 1 GPa N_2, which corresponds to the optimized annealing conditions to recover the ion implantation damage in GaN and to activate rare earth ions.[8,29] Indeed, Lorenz et al.[8] and Roqan et al.[29] established that the efficient optical activation of Eu implanted GaN films can be achieved by postimplantation annealing at high temperatures (>1000 °C) and ultrahigh nitrogen pressures (1 GPa). The samples under study consist of one as-grown diode structure cleaved into four pieces: one as-grown piece kept as a reference (denoted as "as-grown"), two other pieces implanted with the different fluences and then annealed at HTHP (Eu14 for the fluence 1×10^{14} Eu·cm^{-2} and Eu15 for the fluence 1×10^{15} Eu·cm^{-2}) and another as-grown piece only submitted to HTHP annealing (denoted as HTHP). From XRD analysis, we demonstrated that the HTHP annealing at 1400 °C promotes an almost complete recovery of the crystal structure after Eu implantation.[27] In this work, RT Raman spectroscopy measurements (HR800 system) were performed under 325 and 442 nm laser excitations in backscattering configuration. The Eu as-implanted samples (denoted as "as-imp") were only analyzed by Raman spectroscopy in order to study the effects of implantation and HTHP annealing on the structural properties. Steady state PL spectroscopy as a function of temperature (from 14 K to RT) was performed using a coldfinger helium cryostat. The 325 nm line of a cw He−Cd laser (power density $I_0 < 0.6$ W.cm^{-2}) was used as excitation source, corresponding to the energy of ~3.8 eV, above the GaN and $Al_{0.14}Ga_{0.86}N$ bandgaps. The samples' luminescence was dispersed by a SPEX 1704 monochromator (1 m, 1200 g·mm^{-1}) and detected by a cooled Hamamatsu R928 photomultiplier. PL excitation (PLE) and PL spectra were recorded at RT using a Fluorolog-3 Horiba Scientific modular apparatus with a double additive grating scanning monochromator

DOI: 10.1021/acsanm.8b00612
ACS Appl. Nano Mater. XXXX, XXX, XXX−XXX

(2 × 180 mm, 1200 g·mm^{-1}) in the excitation channel and a triple grating iHR550 spectrometer (550 mm, 1200 g·mm^{-1}) coupled to a R928 Hamamatsu photomultiplier for detection. A 450 W Xe lamp was used as excitation source. The measurements were carried out using the front face acquisition geometry and the presented spectra were corrected for the spectral response of the optical components and the Xe lamp.

RESULTS AND DISCUSSION

Raman Spectroscopy. It is known that Raman spectroscopy is extremely sensitive to the damage created by ion implantation and successfully used to study: the structural properties of GaN implanted with various RE ions,[30] HTHP annealing of ion-implanted GaN films,[31,32] as well as structural depth profile in ion implanted GaAs[33] and rapid thermal annealing (RTA) impurity-enhanced interdiffusion in GaAs/AlGaAs QWs.[34,35] Moreover, in GaN and GaN-related alloys, the phonons were proved to be an efficient tool for monitoring the crystalline quality and strain state.[36−38] Figure 1a shows Raman spectra of the as-implanted samples with both fluences recorded using the 325 nm excitation. It is worth mentioning that the as-grown and HTHP samples were not included since they exhibit a strong photoluminescence under the incidence of the 325 nm He−Cd laser line, which prevented the observation of the phonon modes system. Figure 1a shows that the Raman spectra of as-implanted samples exhibit: (i) the Brillouin zone (BZ) center phonon lines E_2^h and A_1(LO), whose intensities decrease and broadenings increase with the Eu fluence and (ii) disorder-activated Raman scattering lines (∼300 and ∼676 cm^{-1} indicated by asterisks), as reported in refs 30 and 39. Indeed, it is known that ion implantation increases the defect density;[31,32] therefore lifting the wavevector conservation of the first order Raman scattering process, which was demonstrated to be closely related to the GaN calculated phonon density of states DOS function,[40,41] in good agreement with our results. Figure 1a. Figure 1b and c show the Raman spectra (in a logarithmic scale) for both Eu as-implanted and Eu14 and Eu15 samples performed using the 325 and 442 nm laser excitations. As stated above, the Eu-profile simulation suggested a maximum ion penetration depth of ∼120 nm,[27] and according to the present diode structure, the use of the 325 nm laser excitation is expected to probe only the first ∼70 nm composed of Mg-doped GaN. For both Eu14 and Eu15 samples, the spectra are dominated by E_2^h and a broad quasi-LO phonon. It is clearly seen that after HTHP (red curve), the first order phonon process at the BZ center becomes predominant, which is consistent with the recovery of the crystalline structure, also corroborating the XRD results in ref 27. The detection of E_2^h, even under GaN resonant excitation conditions, is a clear indication that the near-band-edge (NBE) emission at RT has lower intensity in the Eu14 and Eu15 samples than in the as-grown and HTHP samples. For the Mg nominal doping levels (1−5 × 10^{17} cm^{-3}) of the studied diode structure, the observed broadening of quasi-LO is more likely due to the superposition of E_1(LO) and A_1(LO),[42] rather than a plasmon-phonon coupling,[43] unless there are free carriers generated by implantation.

By using the 442 nm excitation, out of GaN bandgap resonance excitation conditions, the obtained Raman spectra (magenta curves) are dominated by the E_2^h (∼569 cm^{-1}) and A_1(LO) (∼734 cm^{-1}) phonon modes of the wurtzite GaN, in agreement with the reported results in the backscattering configuration for relaxed *c*-plane GaN.[40,44] The detection of the sapphire substrate phonon modes (shown by "S") indicates that all the diode structure is being probed by using the 442 nm excitation wavelength, hindering the identification of the signal from the individual layers. Accordingly, a higher contribution from the GaN layers underneath the AlGaN/GaN SL is expected.

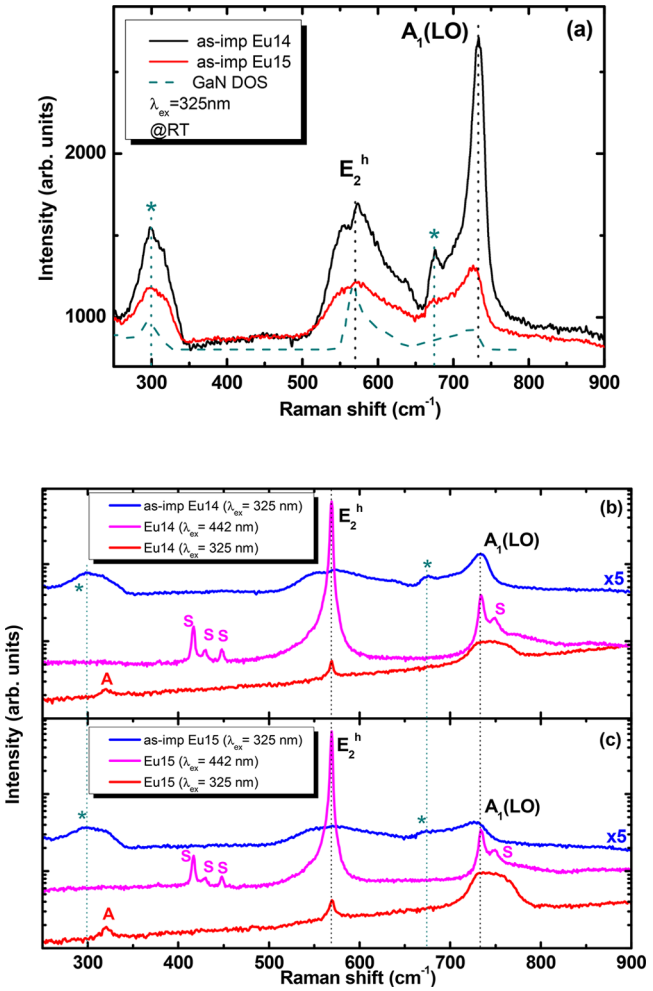

Figure 1. (a) RT Raman spectra of the as-implanted samples with both Eu fluences using laser excitation of 325 nm. The calculated phonon density of states DOS function[40] is included for comparison. RT Raman spectra of the (b) as-implanted Eu14 and Eu14 and (c) as-implanted Eu15 and Eu15 samples using laser excitations of 325 and 442 nm. The asterisks indicate the disorder-activated Raman scattering lines. S indicates the sapphire substrate vibrational modes and A is an artifact.

Photoluminescence. Figure 2 presents 14 K (a) and RT (b) PL spectra of the studied samples, obtained using the 325 nm laser line excitation. The observed PL intensity modulation is related to Fabry−Perot optical interference because of the refractive index contrast of the different layers within the diode structure. Such fringes prove that the interfaces between the constituent layers are smooth and uniform not only for the as-grown sample, but also for the Eu-implanted samples, indicating that Eu implantation/HTHP annealing did not significantly affect the interface properties of the diode structure. In Figure 2a, the PL spectrum corresponding to the as-grown sample (black line) exhibits GaN NBE emission consisting of three sharp lines, as well as the donor−acceptor pair (DAP) recombination and their phonon replicas, a blue luminescence band (BL) centered at ∼2.8 eV (∼445 nm), a broad yellow band (YL) at ∼2.2 eV (∼560 nm) and the second order of the three sharp emission peaks. The sharp emission features can be

DOI: 10.1021/acsanm.8b00612
ACS Appl. Nano Mater. XXXX, XXX, XXX−XXX

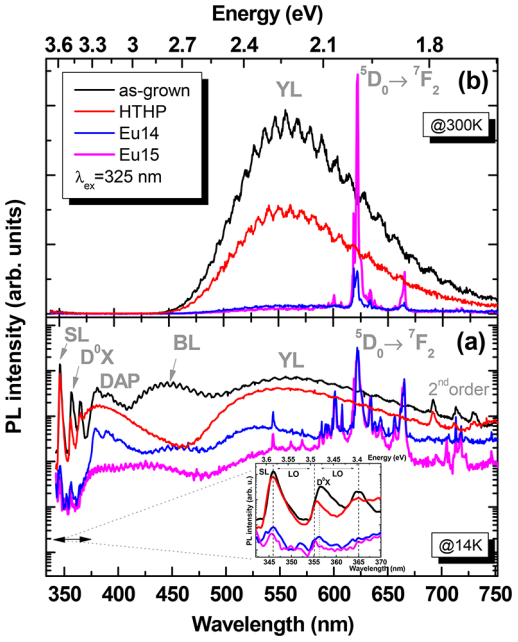

Figure 2. PL of the as-grown, HTHP, Eu14, and Eu15 samples obtained with 325 nm laser excitation at 14 K (a) and at 300 K (b). Inset of (a) shows a magnified 14 K PL below 370 nm.

clearly seen in the GaN NBE energy range (inset of Figure 2a). The most intense emission peak at 3.58 eV (346 nm) is the sharpest one, with a full width at half-maximum (fwhm) of ~13 meV, while the emission peaks at 3.47 eV (357 nm) and 3.39 eV (365 nm) are broader, with fwhm values of 27 and 37 meV, respectively. In addition, a strong decrease of the relative intensities is noticed as the photon energy decreases. Because of its high intensity and sharpness, the feature at 3.58 eV can be attributed to the AlGaN/GaN SL confined excitonic transition from the fundamental electron state to the fundamental heavy-hole state (e_1-hh_1), similarly to what was reported in ref 45. The low fwhm value of the SL transition is consistent with a high crystalline/interface quality and thickness uniformity in our diode structure. As commonly observed in GaN-based structures, for instance GaN epilayers grown on sapphire[46,47] and AlGaN/GaN MQW system,[47,48] inset of Figure 2a indicates the GaN longitudinal optical (LO ~ 91 meV) phonon replica positions with respect to the main emission related to the AlGaN/GaN SL excitonic transition, which is considered as the zero-phonon line. Accordingly, the peak at 3.47 eV could correspond to the superposition of the donor-bound exciton (D^0X) emission originating from the GaN wells/layers and the phonon replica of the SL excitonic transition. While the weak feature at 3.39 eV could originate from additional overlapped two-phonon replicas of the SL excitonic transition and D^0X transitions.

Broad emission bands are well-known to occur in GaN and involve different types of defects. On the one hand, the BL centered at ~2.8 eV (~445 nm), typically observed in Mg-doped GaN films[49] and Mg-doped GaN layers in different heterostructures,[50−52] is usually attributed to Mg-related centers, such as Mg−V_N complexes or isolated Mg_{Ga} acceptors.[53−55] Nevertheless, as the BL emission is also observed in undoped, Mg- and Zn-doped GaN[56] with very similar shape and peak position as the one here reported, the presence of other defects contributing to this band cannot be discarded. However, since the V_N defects are abundantly formed during MOCVD growth,[56] as in our samples, the Mg−V_N complexes could be the origin of the BL[57] observed in the present PL spectra. We believe that this assignment is well-founded because PL measurements as a function of power excitation (BL blue-shifts by ~50 meV for power densities from I_0/10 up to I_0, Figure S2) and temperature (Figure S3) agree well with the PL results of Reshchikov et al.,[49] indicating that the 2.8 eV band blue-shifts by increasing the excitation intensity, and that the corresponding thermal quenching begins at temperatures above 200 K. On the other hand, the broad YL band is peaked at ~2.2 eV, for which the most accepted recombination models involve a DAP or free-to-bound (e-A) transitions. The YL typically involves deep defect levels in intrinsic GaN layers and is often reported as being related to the presence of the native defect V_{Ga} and its complexes.[58,59] In addition, recent theoretical calculations suggest that the YL can also be caused by the carbon impurity (C_N) or its complex with oxygen (C_NO_N).[60−64] Furthermore, it should be noticed that the YL is also affected if GaN is intentionally doped. Indeed a substantial increase of the YL intensity was found using several dopants such as Si or Mg, as reported by Reshchikov et al.[56] In Mg-doped GaN, first-principles calculations predicted the formation of three donor defects: a nitrogen vacancy, interstitial Mg, and the N-vacancy-Mg complex.[65]

By comparing the as-grown and HTHP samples, it can be seen that the low temperature PL spectrum is slightly affected by HTHP annealing (red line in Figure 2a), especially around the GaN DAP and BL spectral regions. Regarding the DAP region, a slight decrease of the PL intensity is obtained after HTHP annealing. A similar evolution of the DAP was recently obtained for MOCVD Mg-doped GaN layers annealed above 870 K.[66] The broad band observed for the HTHP sample, around ~3.26 eV (~380 nm), could be associated with two hypothesis: (i) unresolved DAP recombination accompanied by an important decrease of the BL intensity or to (ii) the blue-shift of the BL, overlapping with the DAP recombination. For the first one, Nakamura et al.[67] reported a decrease of the blue emission (~450 nm) intensity in Mg-doped GaN films for annealing temperatures above 700 °C, which was attributed to the thermal dissociation of the GaN. For the second hypothesis, the BL blue-shift could be understood in terms of Mg diffusion from the GaN p-type layer to the AlGaN/GaN SL after annealing. Indeed, Mg-doped $Al_xGa_{1-x}N$ samples[57,68,69] showed that the peak position of the defect-related band blue-shifts almost linearly with increasing Al content. Since Raman and NBE PL spectra clearly show the presence of a good quality GaN layers after HTHP, we believe that the second possibility is more likely to occur in our samples with nominal AlN content of ~14% in the AlGaN/GaN SL.

After Eu implantation and HTHP annealing, the SL transition at 3.58 eV, as well as the D^0X emission intensities (and their phonon replicas), are reduced by approximately 2 orders of magnitude. As will be further discussed, this indicates that the Eu implanted ions have effectively reached the AlGaN/GaN SL region, but did not strongly affect the diode structure. This is in a very good agreement with our structural study.[27]

For the sample implanted with the lowest fluence (Eu14), the ultraviolet DAP recombination is still observed even after HTHP annealing. In addition, the intensity of the DAP and the defect-induced BL and YL broad band intensities have decreased by 1 order of magnitude, due to the lattice damage induced by the implantation processes. In the energy range below 2.29 eV (above 543 nm), the sharp luminescence lines, characteristic of the Eu^{3+} intra-4*f* shell transitions with the

DOI: 10.1021/acsanm.8b00612
ACS Appl. Nano Mater. XXXX, XXX, XXX−XXX

most intense emission corresponding to the $^5D_0 \rightarrow {}^7F_2$ transition (~621 nm), are well resolved and dominate the spectrum in Figure 2a. At 14 K, we can conclude that HTHP thermal annealing reduced the implantation-induced defects, recovered some of the native luminescence and optically activated the Eu^{3+} ions. The detailed study related to the Eu^{3+} emission lines and their temperature dependences will be discussed below. Though this sample was subject to HTHP annealing, which could have led to a Mg diffusion from GaN to the AlGaN/GaN SL (as stated above for the HTHP sample), in this case the BL peak position remained unchanged, which suggests that the Eu implantation or the corresponding structural interface damage might have prevented the Mg diffusion into the AlGaN/GaN SL. For the Eu15 sample, besides the decrease of the intensity of the native luminescence, both DAP and BL emissions are seen to broaden due to a lower recovery of the lattice damage with respect to the sample Eu14.

Figure 2b indicates that PL intensity experiences a strong thermal quenching with increasing temperature (from 14 K to RT) in the UV range for all samples. For nonimplanted samples (as-grown and HTHP), only the YL persists at RT. This behavior versus temperature is commonly observed in GaN-based structures.[59] For samples Eu14 and Eu15, an emission overlap of the YL with the Eu^{3+} intraionic luminescence is observed at RT. The thermal quenching of the Eu-related luminescence is much less pronounced when compared to the NBE luminescence, indicating a lower amount of thermally induced nonradiative processes. We have found that, for sample Eu14, the relative intensity of the $^5D_0 \rightarrow {}^7F_2$ transition is strongly decreased when compared with the emission at 14K, while the intensity remains similar for the Eu15 sample, indicating a higher intraionic emission thermal stability for the sample implanted with the highest fluence.

The perceived photoexcited emission color represented by the chromaticity coordinates (Commission Internationale de l'Eclairage CIE 1931, calculated from the corresponding PL spectra) is shown in Figure 3 for different temperatures from 14 to 300 K. For the as-grown sample (squares), the emission color changes from white to yellow, while the HTHP sample (spheres) shows a stable and temperature independent yellow emission. For the Eu14 sample (triangles), the emission changes from orange-red (14 K) to yellow-orange (RT). When the Eu fluence increases up to 1×10^{15} Eu·cm^{-2} (stars), the color emission becomes red and almost independent of temperature, exhibiting higher thermal color stability than the Eu14 sample. We have recently reported that, unlike GaN layers, the use of the 325 nm excitation was found to be the most efficient photoexcitation for providing the perceived red emission in nitride-based diode structure.[70]

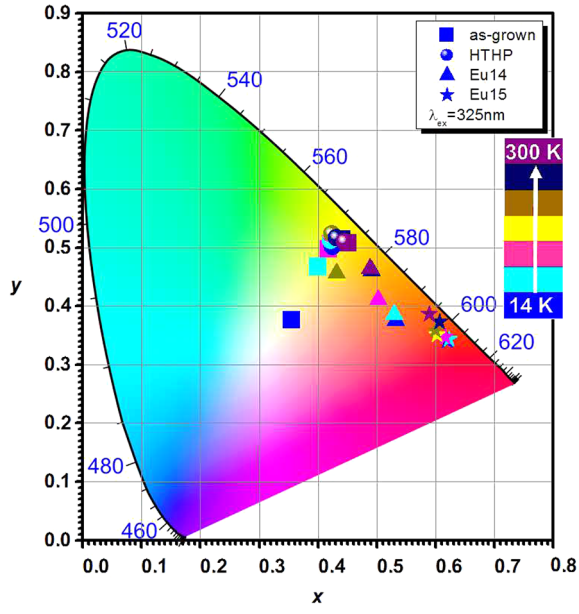

Figure 3. Chromaticity coordinates (CIE 1931) for the different temperatures (14–300 K) of all samples obtained with 325 nm laser excitation.

Photoluminescence Excitation. It is well established that the Eu^{3+} intraionic emission possesses different sensitivities to above and below bandgap excitations, as observed in Eu-implanted GaN layers.[7] Therefore, on the basis of the RT PL spectra in Figure 2b, a detailed study of the population mechanisms occurring at RT in the present diode structure was performed. Figure 4a–d present normalized RT PLE spectra monitored at the maximum of the YL (549 nm) for all samples, and Figure 4e and f present normalized RT PLE spectra monitored at the $^5D_0 \rightarrow {}^7F_2$ transition (621 nm) for Eu14 and Eu15 samples. Combined excitation emission spectra (CEES) for the as-grown, HTHP, Eu14, and Eu15 samples are shown in Figure S4. To get more insight into the different features observed in the PLE spectra, the normalized experimental spectra (black dots in Figure 4a–f) were analyzed using eq 1, following a similar procedure as the one used for AlGaN/GaN MQW photocurrent spectra:[71]

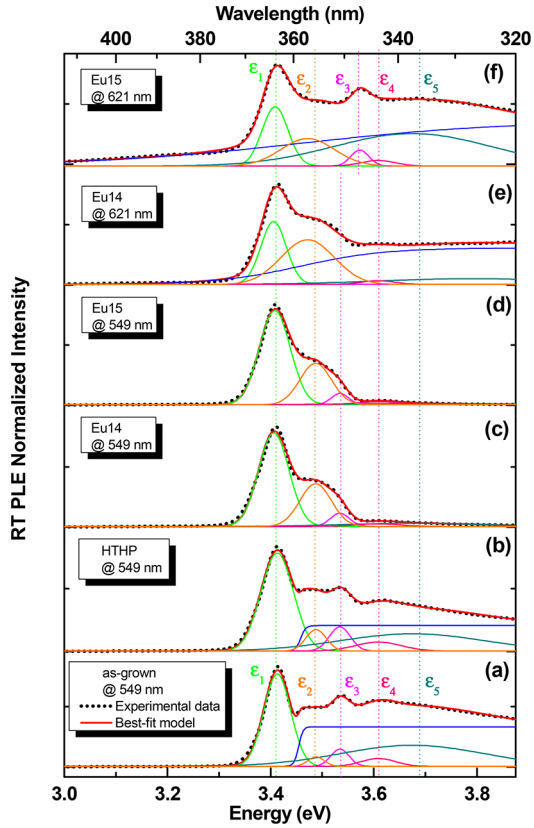

Figure 4. Experimental (black dots) and best-fit calculated using eq 1 (red solid lines) PLE normalized spectra for all the samples monitored at 549 (a–d) and 621 nm (e and f).

DOI: 10.1021/acsanm.8b00612
ACS Appl. Nano Mater. XXXX, XXX, XXX–XXX

$$\mathrm{PLE}(E) = C + \sum_{i=1}^{5} \frac{A_i}{w_i\sqrt{\frac{\pi}{2}}} \exp\left[-2\left(\frac{E-\epsilon_i}{w_i}\right)^2\right] + \frac{A_s}{1+\exp\left[-\left(\frac{E-\epsilon_s}{w_s}\right)\right]} \quad (1)$$

where the terms on the right-hand side correspond respectively to a constant C, a term containing five Gaussian functions, and a term representing the sigmoidal formula. The sigmoidal function was successfully used in InGaN epilayers,[72] InGaN/GaN MQWs,[59] and AlGaN/GaN MQWs[71] to describe the near-band gap absorption, where ϵ_S represents the effective bandgap and w_s a parameter equivalent to the Urbach tailing energy.[72] The quantities C, A_i, A_s, ϵ_i, ϵ_S, w_i, and w_s correspond to the adjustable fitting parameters, with A_i and A_s being the intensities, ϵ_i and ϵ_S the energy positions, and w_i and w_s the broadening parameters (more details can be found in Supporting Information). The best-fit calculated curves using eq 1 are indicated by red lines in Figure 4a–f. In the energy range 3–3.9 eV, the Gaussian excitation bands indicated in Figure 4a–f were tentatively assigned to GaN bulk excitonic transition (ϵ_1), SL excitonic transition (ϵ_2) from the fundamental heavy-hole level to the fundamental electronic level (hh_1-e_1), SL excitonic transition (ϵ_3) from the fundamental light-hole level to the fundamental electronic level (lh_1-e_1), SL excitonic transition (ϵ_4) from the excited light-hole level to the fundamental electronic level (lh_2-e_1), and an additional high-energy structure (ϵ_5). The lines at ϵ_2, ϵ_3, and ϵ_4 energies were assigned, for the as-grown sample, according to the theoretical calculations performed by Bulutay et al.[45] For a well width of ∼2.5 nm, these authors found that the ϵ_2 and ϵ_3 intensities (oscillator strength) are similar, while the one of ϵ_4 is much lower. We should emphasize the fact that the SL transitions are resolved from PLE spectra, even at RT, indicating the high quality of our diode structure. For the AlGaN/GaN MQW system, interband transitions were previously resolved using low temperature PLE[73,74] or partially resolved using RT photocurrent[71] spectroscopy.

It can be seen that the PLE spectrum in Figure 4b monitored at the maximum of the YL (549 nm) is only slightly affected by HTHP annealing (in comparison to as-grown sample in Figure 4a), where a slight increase of the ϵ_2 intensity and a decrease in the sigmoidal function intensity are observed. After Eu-implantation with both fluences and HTHP annealing (Figure 4c and d), the PLE spectral shape has significantly changed. More specifically, no sigmoidal term was included in the fit function, probably due to the created defects that act as nonradiative recombination centers. In addition, a noticeable increase of the fwhm of the ϵ_2 transition (hh_1-e_1) is found in comparison to the one of the as-grown sample which is due to disorder effects induced by the implantation and HTHP annealing. These observations confirm once again that the Eu implanted ions have reached the AlGaN/GaN SL region and have slightly affected the SL structure. Concerning the PLE spectra monitored at the $^5D_0 \rightarrow {}^7F_2$ transition (621 nm) of the Eu14 sample (Figure 4e), no significant change is observed below 3.55 eV when compared to the PLE monitored at 549 nm for the same sample, (Figure 4c). However, above 3.55 eV, an increase of the intensity of the ϵ_3 and ϵ_4 transitions is observed. For the highest fluence sample, Eu15, the PLE (monitored at 621 nm) shows an enhanced onset absorption below the bandgap and a blue-shifted ϵ_3 feature, as seen in Figure 4f. On the one hand, the subgap absorption is known to occur in ion implanted semiconductors such as Eu-implanted GaN,[7,75,76] indicating an excitation pathway involving defect levels or complexes associated with the implanted ion. In our case, the Eu15 sample represents the most defective material and therefore contains the largest number of states inside the bandgap, which explains the higher absorption below 3 eV when compared to the as-grown and HTHP samples. On the other hand, a higher ϵ_3 energy value was needed to better describe the PLE of the Eu15 sample. It is known that, in quantum wells, the presence of impurities or implantation damage, or both, can enhance the interdiffusion responsible for the potential profile change at the interface.[35] The effect of the interdiffusion on the electron and hole quantized states in the well was found to be an effective downshift with respect to the bottom of the bands,[35] inducing a blue-shift of the interband transition energies as a result of the changes in confinement and composition energy.[77] Accordingly, the observed blue-shift of the ϵ_3 feature, assigned to the SL excitonic transition from the fundamental light-hole level to the fundamental electronic level (lh_1-e_1) might be due to interdiffusion effect induced by Eu implantation. Since the PLE is monitored on the most intense Eu^{3+} intra-4*f* shell transitions (621 nm) in the Eu15 sample (Figure 4f), an enhanced effect of the Eu implantation and HTHP in the SL structure is expected to be observed, which could not be well resolved when the PLE is monitored at the YL maximum (549 nm) for the same sample (Figure 4d). It should be emphasized that, as observed in Figure 2a for the Eu15 sample, the YL was found to have the lowest intensity when compared to the other samples, probably because of the created defects that act as nonradiative recombination centers. Consequently, the PLE analysis demonstrates that, in addition to the GaN subgap excitation, an energy transfer between the AlGaN/GaN SL excitons and the Eu^{3+} ions occurs, therefore enlarging the excitation pathways for the red luminescence in these structures.

Temperature-Dependent $^5D_J \rightarrow {}^7F_J$ Transitions. It is well established that, in addition to the perturbations introduced by electrostatic interaction of the electrons in the 4*f* shell and by the spin–orbit coupling, the crystal-field perturbation introduced by the host material (GaN and $Al_{0.14}Ga_{0.86}N$) destroys the spherical symmetry of the free-ion (Eu^{3+}), leading to a splitting of the $^{2S+1}L_J$ terms in a number of crystal-field (or Stark) levels.[78] In the trigonal case (as for GaN[18] and AlN[79]), where the RE ion predominantly occupies the Ga^{3+} substitutional sites in the C_{3v} symmetry, the $^7F_1$ level splits into a doublet (E) and a singlet (A) (i.e., A+E), while the $^7F_2$ splits into two doublets E and a singlet A (i.e., A+E+E). A lowering of symmetry results in a relaxation of the selection rules and an increase of the number of allowed transitions[78] to a maximum of (2*J* + 1), corresponding to 3 and 5, for the $^7F_1$ and $^7F_2$ multiplets, respectively. Furthermore, no crystal field splitting is allowed for levels with *J* = 0 (e.g., $^7F_0$, $^5D_0$).

In order to perform a detailed study of the Eu-related red luminescence from the $^5D_J \rightarrow {}^7F_J$ multiplets, the PL temperature dependences are represented around the $^5D_0 \rightarrow {}^7F_0$ (Figure 5a and b), $^5D_0 \rightarrow {}^7F_1$ (Figure S5a and b), and $^5D_0 \rightarrow {}^7F_2$ (Figure 6a and b) transitions for both Eu implanted and annealed samples. The different Eu^{3+} emission lines (also summarized in Table 1) are denoted as (Q1, Q2, Q3), (R1–R6 in Figures S5a and b) and (P1–P9), for the $^5D_0 \rightarrow {}^7F_0$, $^5D_0 \rightarrow {}^7F_1$, and $^5D_0 \rightarrow {}^7F_2$ transitions, respectively. Table 1 summarizes all the Eu^{3+} intraionic transitions observed in the PL of our structure at

DOI: 10.1021/acsanm.8b00612
ACS Appl. Nano Mater. XXXX, XXX, XXX–XXX

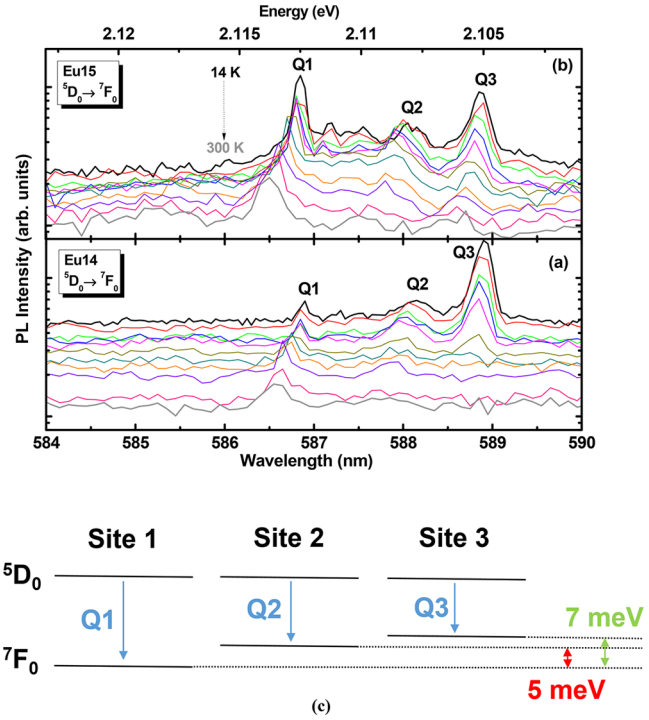

Figure 5. High-resolution temperature-dependent PL for the Eu14 (a) and Eu15 (b) samples around the $^5D_0 \rightarrow {}^7F_0$ region. (c) Observed transitions and the corresponding receiving $^7F_0$ states of the three Eu sites.

14 K, the reported ones for Eu^{3+} in GaN layers and nanowires (NWs), Eu and Mg codoped GaN layers, *w*-AlN single crystals, and the corresponding assignments.[1,8,12,16,25,79−85] A careful comparison of our results with these reports allowed to tentatively provide the Eu^{3+} intraionic transition assignments of the present diode structure. Both Eu14 and Eu15 samples exhibit the same Eu^{3+} intraionic transitions (within the experimental error of 0.10 nm), with different relative intensities, except resolved transitions in the $^5D_0 \rightarrow {}^7F_4$ region for Eu15 sample.

From Table 1, it can be seen that different Eu emission lines are resolved depending on the sample growth and doping techniques. In the present diode structure, numerous Eu^{3+} intraionic lines are observed in the spectral range: 580−730 nm. Most of the Eu-related emission peak positions obtained for the present diode structure (such as Q1−Q3 and P1−P9) have similar values as those obtained for GaN, either by in situ doping[82] or ion implantation,[81,85] indicating that the Eu is optically active within the first 120 nm of the structure composed of GaN:Mg top layer and Si-doped AlGaN/GaN SL. Indeed, it was demonstrated that increasing the AlN content in AlGaN alloys induces a red-shift of the Eu^{3+} related emission.[22,86,87] However, for AlN content of 0.14, as it is the case for the AlGaN layers in the present SL, the red-shift is negligible, preventing the possibility to distinguish whether the ions were activated in GaN, AlGaN, or both.

*$^5D_0 \rightarrow {}^7F_0$ Transition. The induced electric dipole "sensitive" $^5D_0 \rightarrow {}^7F_0$ transition is forbidden following the standard Judd−Ofelt theory.[78] The fact that this transition is observed in our case is a result of the breakdown of the selection rules (i.e., C_{3v} local symmetry destroyed) due to the distorted/strained original (GaN and $Al_{0.14}Ga_{0.86}N$) unit cells after the Eu^{3+} implantation. The $^5D_0 \rightarrow {}^7F_0$ transition intensity is approximately 2 orders of magnitude lower than the one of the $^5D_0 \rightarrow {}^7F_2$ transition. In addition, due to the singlet character of the $^7F_0$ fundamental and $^5D_0$ excited levels, the number of the observed $^5D_0 \rightarrow {}^7F_0$ transitions corresponds to the number of non equivalent active sites in the Eu implanted sample, if accidental overlaps are omitted.[78,88,89,82]

In Figure 5a and b, around the $^5D_0 \rightarrow {}^7F_0$ region at 14 K, three transitions are well resolved for both Eu-implanted samples: Q1, Q2 and Q3, respectively peaked at 586.85 (2.113 eV), 588.05 (2.108 eV), and 588.85 nm (2.106 eV). It should be emphasized that the Q1, Q2, and Q3 transitions are not originating from phonon-assisted transitions, for which the energy separation should be ∼10.5 meV. Accordingly, at least three different active sites are created by the Eu implantation in the present diode structure. Figure 5c shows a tentative representation (not to scale) of the observed transitions and the corresponding receiving $^7F_0$ states of the three Eu sites. Table 2 summarizes the $^5D_0 \rightarrow {}^7F_0$ transitions (top) and relative estimated energy levels (bottom) derived from our PL spectra, found to be in good agreement with previous reports.[84,82] The site Q3 (Q1) is very similar to the prominent transition ∼588.9 nm (∼586.9 nm) recorded at 13 K (100 K), and attributed to the Eu1(Mg) (Eu0) defect configuration in Eu-implanted and annealed Mg-doped GaN layers.[16] We remind that when cooling down such samples, the Eu0 line intensity increases up to 200 K, then vanishes below 30 K and is replaced by the Eu1(Mg) lines. This behavior is the photochromic switch, demonstrating the structural instability of GaN(Mg) at low temperature.[14,15,88] It is important to emphasize that the studied samples are subject to the same HTHP annealing conditions as the ones in ref 16, however, the simultaneous occurrence of both site configurations Eu0 and Eu1(Mg) at 14 K implies that the photochromic switch is not observed, which could be due to the lower Mg concentration or to the presence of the SL in the present diode structure. Furthermore, Table 1 suggests that the site Q2 can be associated with MS2[80] and OMVPE7[83] sites in Eu-doped GaN, where MS2 is known to be dominantly present in ion-implanted samples.[80]

In (Eu, Mg) codoped GaN layers,[12] only one peak (∼586.8 nm) was observed in the $^5D_0 \rightarrow {}^7F_0$ region at 180 K, attributed to the Eu−Mg site. According to Lee et al.,[12] even if several sites are created by (Eu, Mg) codoping in GaN, increasing the temperature selectively enhances only one site (Eu−Mg site). Indeed, this statement is in good agreement with our results, since at RT it can be seen that the most intense emission corresponds to the Q1 transition for both Eu-implanted and annealed diode structure. In the case of Mg, Si and Eu codoping of GaN layers, Mishra et al.[25] observed similar spectra in the $^5D_0 \rightarrow {}^7F_0$ region, with an enhanced peak intensity at ∼586.8 nm with respect to the other peaks, that the authors related to the fact that Si and Mg codoping activates a particular Eu site.

At RT, the dominance of the Q1 site is clearly seen independently of the Eu fluence (also in Figure S6). This result is in good agreement with Singh et al.,[16] who recently reported that the red emission at RT of implanted and annealed samples comes from a single center, suggesting a selective attraction between Eu and Mg atoms in GaN during annealing.

*$^5D_0 \rightarrow {}^7F_1$ Transition. The magnetic dipole $^5D_0 \rightarrow {}^7F_1$ transition is known to be independent of the environment of the Eu^{3+} ion.[78] The study of the $^5D_0 \rightarrow {}^7F_1$ transition is very important and its crystal field analysis was successfully used to solve issues related with site multiplicity of Eu^{3+} emission in

DOI: 10.1021/acsanm.8b00612
ACS Appl. Nano Mater. XXXX, XXX, XXX−XXX

Table 1. Eu^{3+} ($4f^6$) Intraionic Transitions Observed in the Eu Implanted Diode Structure and Corresponding Assignments $^5D_{0,1} \rightarrow {}^7F_{0,1,2,3,4}$

		this work (14 K)		ref 16 (13 and 100 K)	ref 8 (20 K)	ref 80			ref 82 (RT)		ref 25 (15 K)			
		10^{14} Eu ions·cm^{-2} implanted AlGaN/GaN diode structure	10^{15} Eu ions·cm^{-2} implanted AlGaN/GaN diode structure	10^{13}–10^{14} Eu ions·cm^{-2} implanted GaN layers (Mg codoping)	10^{13}–10^{15} Eu ions·cm^{-2} implanted GaN layers	Eu-in-situ-doped and implanted GaN samples	refs 81, 85 (14 K)		Eu-doped in situ GaN layers		10^{14} Eu ions·cm^{-2} implanted GaN layers (Mg and Si codoping)		ref.79 (11 K)	other refs
transitions (nm)	peak label	peak positions ±0.10 nm		assignment	assignment	assignment	5×10^{13} Eu ions·cm^{-2}implanted GaN NWs[a]	3×10^{15} Eu ions·cm^{-2} implanted GaN NWs[a]	assignment		assignment		Eu-doped *in situ* AlN single crystals	assignment
$^5D_0 \rightarrow {}^7F_0$									585.2					
	Ql	586.90	586.85	586.9 Eu0		587.0 MS_3					586.8			587.95 OMVPE$_7$[1]
	Q2	588.10	588.05			587.9 MS_2			588.5	sIII	589.0			
	Q3	588.90	588.85	588.9 Eu1(Mg)		588.8 MainS			589.9				590.34	588.76 OMVPE$^6_1$
									591.9					
$5D_0 \rightarrow 7F_1$	Rl	598.85	598.80				598.8	598.8						
	R2	600.60	600.60	600.8 Eu0/Eu1(Mg)			600.4		600.8	sIV				
				601.3 Eu1(Mg)			601.1	601.1						
	R3	602.30	602.25	602 7 Eu0/Eu1(Mg)			602.2	602.3						
									604.6				602.49	
	R4	605.85	605.85						606.1	sII			604.35	
	R5	607.20	607.10											
	R6	607.95	607.90						607.8	sI				
$^5D_0 \rightarrow {}^7F_2$		($^5D_0 \rightarrow {}^7F_2$ or $^5D_1 \rightarrow {}^7F_4$)									615.1			
	P1	617.45	617.45		617.2 Eu2	617.2 MS_7								
	P2	618.90	618.90	618.9 Eu0	618.7 Eu2	618.9 MS_4	618.8	618.8	618.8	sIII	619	Eu, Mg		619 Eu–Mg (A)[2]
	P3	619.50	619.40	619.5 Eu0	619.3 Eu2	619.6 MS_4		619.4						
				620.6 Eu1(Mg)					620.6	sII	620.3	Eu, Mg		620.3 site-A[3]
	P4	621.00	620.95	620.9 Eu1(Mg)	620.8 Eu1/Eu2	621.0 MS_2	620.8	620.9						
	P5	621.85	621.80	621.8 Eu1(Mg)	621.7 Eu1/Eu2	621.9 MS_8	621.7	621.7						622 OMVPE$_4$(B)[2]
	P6	622.70	622.70	622.7 Eu1(Mg)	622.5 Eu1	622.6 MainS	622.6	622.7	622.5	sI				622.3 site-B[3]
													623.95	
													624.49	
	P7	632.90	632.75			632.7 MS_4	632.8	632.8						
	P8	633.90	633.85	633.9 Eu1(Mg)		633.9 MS_3								633.9 site-C[3]
	P9	634.60	634.50			634.3 MainS	634.1	634.2						
												635.79		
$^5D_0 \rightarrow {}^7F_3$									656.1	sIV				

ACS Appl. Nano Mater. XXXX, XXX, XXX−XXX
DOI: 10.1021/acsanm.8b00612

Table 1. continued

		this work (14 K)		ref 16 (13 and 100 K)	ref 8 (20 K)	ref 80			ref 82 (RT)		ref 25 (15 K)			
		10^{14} Eu ions·cm^{-2} implanted AlGaN/GaN diode structure	10^{15} Eu ions·cm^{-2} implanted AlGaN/GaN diode structure	10^{13}–10^{14} Eu ions·cm^{-2} implanted GaN layers (Mg codoping)	10^{13}–10^{15} Eu ions·cm^{-2} implanted GaN layers	Eu-in-situ-doped and implanted GaN samples	refs 81, 85 (14 K)		Eu-doped in situ GaN layers		10^{14} Eu ions·cm^{-2} implanted GaN layers (Mg and Si codoping)		ref.79 (11 K)	other refs
transitions (nm)	peak label	peak positions ±0.10 nm		assignment	assignment	assignment	5×10^{13} Eu ions·cm^{-2}implanted GaN NWs[a]	3×10^{15} Eu ions·cm^{-2} implanted GaN NWs[a]	assignment		assignment		Eu-doped *in situ* AlN single crystals	assignment
		656.00	655.90					656.5						
		656.75	656.75											
							660.5							
		662.00	662.05			661.8 MainS	662.1	662.1	662.0	sIII				
		664.00	663.90			663.8 MainS	664.0	664.0	662.7				664.03	
		665.30	665.20			665.2 MainS	665.2	665.2	665.2	sI			665.74	
													667.33	
$^5D_0 \rightarrow {}^7F_4$			694.70											
			704.70											
		706.75	706.70						706.9	sIV			707.21	
													709.77	
		713.25	713.20						713.1	sIII			713.84	
			716.70						716.8	sI				
		718.25	718.20											
													719.71	
		722.25	722.70											
$^5D_1 \rightarrow {}^7F_1$									541.2					
		543.75	543.70	543.4 Eu1(Mg)										543[4]
				543.5 Eu1(Mg)					544.3				544.87	
				543.9 Eu1(Mg)									546.16	
				544.0 Eu1(Mg)					546.7				546.38	
				544.3 Eu1(Mg)									562.01	
				545.2 Eu1(Mg)										
$^5D_0 \rightarrow {}^7F_2$									553.1					
									558.3					
		560.25	560.20	559.5 Eu1(Mg)										
				559.6 Eu1(Mg)										
				559.8 Eu1(Mg)										
				560.0 Eu1(Mg)										
				560.4 Eu1(Mg)									562.18	
				560.5 Eu1(Mg)									562.52	

ACS Appl. Nano Mater. XXXX, XXX, XXX−XXX
DOI: 10.1021/acsanm.8b00612

Table 1. continued

		this work (14 K)		ref 16 (13 and 100 K)	ref 8 (20 K)	ref 80			ref 82 (RT)	ref 25 (15 K)		
		10^{14} Eu ions·cm^{-2} implanted AlGaN/GaN diode structure	10^{15} Eu ions·cm^{-2} implanted AlGaN/GaN diode structure	10^{13}–10^{14} Eu ions·cm^{-2} implanted GaN layers (Mg codoping)	10^{13}–10^{15} Eu ions·cm^{-2} implanted GaN layers	Eu-in-situ-doped and implanted GaN samples	refs 81, 85 (14 K)		Eu-doped in situ GaN layers	10^{14} Eu ions·cm^{-2} implanted GaN layers (Mg and Si codoping)	ref.79 (11 K)	other refs
transitions (nm)	peak label	peak positions ±0.10 nm		assignment	assignment	assignment	5 × 10^{13} Eu ions·cm^{-2}implanted GaN NWs[a]	3 × 10^{15} Eu ions·cm^{-2} implanted GaN NWs[a]	assignment	assignment	Eu-doped *in situ* AlN single crystals	assignment
				561.2 Eu1(Mg)							563.80	
				561.3 Eu1(Mg)							571.80	
		570.75	570.70	570.9 Eu1(Mg)							571.91	
											593.50	
$^5D_1 \rightarrow {}^7F_3$									586.6			
									589.9			
		592.00	592.00									
		592.90	592.85						592.5 sI			
											593.80	
											594.52	
		594.70	594.70								594.74	
		595.85	595.85								595.80	
											596.08	
											597.15	
											597.32	
											599.60	
											599.92	

[a]Nanowires (NWs). [b]Ref 83. [c]Ref 12. [d]Ref 1. [e]Ref 84.

DOI: 10.1021/acsanm.8b00612
ACS Appl. Nano Mater. XXXX, XXX, XXX−XXX

Table 2. $^5D_0 \rightarrow {}^7F_0$ Transitions (Top) and Relative Estimated Energy Levels (Bottom) Derived from Our PL Spectra (±1 meV)

site $^5D_0 \rightarrow {}^7F_0$	energy (eV) (this work)		
site 1	2.113		
site 2	2.108		
site 3	2.106		
level	energy (eV) (this work)	energy (eV) (ref 82)	energy (eV) (ref 84)
$^5D_0$	0	0	0
$^5D_1$	0.210	0.227	0.210
$^7F_0$	0	0	0
$^7F_1$	0.043	0.056	0.032
$^7F_2$	0.105	0.104	0.102
$^7F_3$	0.223	0.232	0.232
$^7F_4$	0.329	0.366	0.352

(Eu, Mg) codoped GaN.[88] As stated above, in accordance with the C_{3v} symmetry, the state with $J = 1$ ($^7F_1$) splits into 2 levels: a doublet (E) and a singlet (A). The observation of more than two transitions, labeled as R1−R6 in Figure S5, is an additional indication of the presence of more than one active site in the Eu implanted and annealed diode structure.

$^5D_0 \rightarrow {}^7F_2$ Transition. The $^5D_0 \rightarrow {}^7F_2$ transition is the so-called "hypersensitive transition", the intensity of which is much more influenced by the local symmetry of the Eu^{3+} ion and the nature of the ligands than the intensities of the other electric dipole transitions. It has been pointed out that the trivalent RE ions in GaN assume a substitutional Ga site being in a relaxed C_{3v} symmetry,[89,18] however, other incorporation sites are also possible.[82] The observation of fine structures in the PL spectra of the main $^5D_0 \rightarrow {}^7F_2$ transition suggests a J-degeneracy lifting of the $^7F_2$ multiplets and lower site symmetry than C_{3v}. We have discussed above the possibility of at least three different sites in the present Eu-implanted and annealed diode structure. Since the Eu^{3+} dopants may experience a variety of local environments (pure substitutional Ga site, Eu^{3+} clustering, regions devoid of Eu^{3+} substitutions, and the presence of native defects and impurities) associated with a complex fine-structure spectra for the $^5D_0 \rightarrow {}^7F_2$ region (Figure 6a and b), and a higher probability of J-mixing, a similar approach to the one used for R4, R5, and R6 transitions (Figure S5) for assigning the different sites cannot be easily applied. However, we could assign the observed transitions to the Eu0 and Eu1(Mg) defect configurations, in comparison to the different sites reported in the literature (as indicated in Table 1).

Figure 6c shows the temperature dependence of the PL intensity for the peak P1 (617.45 nm) and peaks P2−P9, in the $^5D_0 \rightarrow {}^7F_2$ region for Eu15 sample. The same behavior was found for sample Eu14 (not shown). As can be seen in Figure 6c, the PL intensity of the P2−P9 emission lines decreases with temperature, but with different quenching factors. Interestingly, the P1 peak (~617.5 nm) PL intensity shows a very different temperature behavior, with an increase up to ~120 K, followed by a decrease up to RT, suggesting the presence of thermally activated population mechanisms. A similar PL peak was observed in GaN:Eu,[90,76] with a similar temperature behavior attributed to a possible selective population of Eu^{3+}-related complex with increasing temperature.[91] A peak at 617.6 nm was also recorded with enhanced intensity in $Al_{0.11}Ga_{0.89}N$:Eu, with respect to GaN:Eu, using above bandgap excitation.[24]

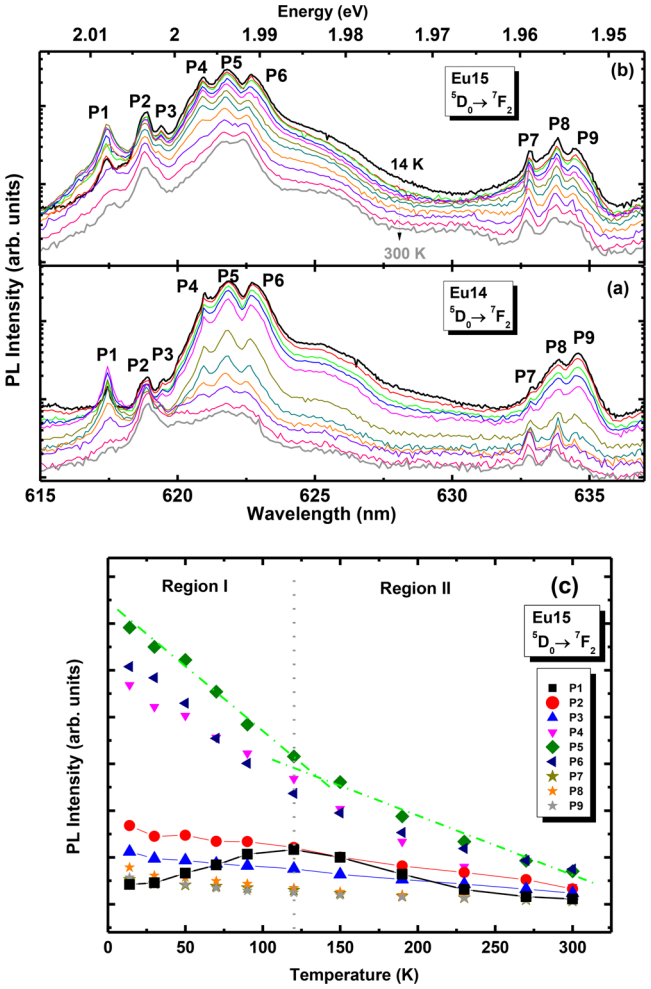

Figure 6. High-resolution temperature dependence PL for the Eu14 (a) and Eu15 (b) samples around the $^5D_0 \rightarrow {}^7F_2$ region. (c) Temperature dependence of the PL intensity for the peak P1 (617.45 nm) and P2 to P9, in $^5D_0 \rightarrow {}^7F_2$ region for Eu15 sample.

In this work, the obtained peculiar temperature behavior of the P1 peak intensity allows to define two regions I and II for temperatures below 120 K and above 120 K, respectively. Both regions are limited by the vertical dotted line, as shown in Figure 6c. It can be clearly seen that each of the peaks P1 to P6 exhibit different quenching regimes in both regions, described by different slopes (such as the one represented in dash-dotted line for the P5 peak). According to the assignments in Table 1, P1 is described by Eu2 site, P2 and P3 are described by the Eu0 defect configuration, while P4, P5, and P6 are described by the Eu1(Mg) defect configuration. When the temperature increases up to ~120 K, the intensity of P1 increases and those of P4−P6 peaks rapidly decrease, while those of P2 and P3 decrease smoothly. This indicates that substitutional Eu impurity (Eu_{Ga}) Eu2 site is favored over Eu−Mg defect at temperatures lower than ~120 K. When the temperature increases further in region II, the intensity of P1 starts to decrease and the slope of the thermal quenching of P2−P6 is lower when compared to region I.

In summary, our PL and PLE results revealed that three main nonequivalent optically activated Eu^{3+} sites are favored in the diode structure under the present ion implantation and annealing conditions, which are predominantly populated through energies above GaN and $Al_{0.14}Ga_{86}N$ bandgaps.

DOI: 10.1021/acsanm.8b00612
ACS Appl. Nano Mater. XXXX, XXX, XXX−XXX

In contrast to GaN layers,[2,87] the perceived Eu^{3+} red emission observed at room temperature was found to be strongly sensitive to the GaN above bandgap excitation, suggesting that additional energy transfer between the AlGaN/GaN superlattice excitons and the Eu^{3+} ions occurs, therefore widening the excitation pathways for the red luminescence.

CONCLUSIONS

The effects of the HTHP annealing and europium implantation followed by HTHP annealing on the AlGaN/GaN diode structure were studied by optical techniques. We have shown that the diode structure exhibits a stable crystalline quality after HTHP annealing at 1400 °C in 1 GPa N_2. The photoluminescence response was found to be only slightly affected by the heat treatment conditions in the near band edge region. After Eu implantation and HTHP annealing, the spectroscopic analysis clearly shows that the ions reached the first AlGaN/GaN quantum wells of the diode structure. We have shown that HTHP thermal annealing has removed implantation defects, recovered some of the as-grown luminescence and optically activated the Eu^{3+} ions. A model was built for the photoluminescence excitation response based on the different excitation bands originated from the materials present in the diode structure, indicating that an energy transfer between the AlGaN/GaN superlattice excitons and the Eu^{3+} ions occurs, therefore enlarging the excitation pathways for the ion's red luminescence. In addition, Eu^{3+} luminescence was observed not only with above but also with below GaN bandgap excitation, corresponding to a broad excitation band overlapped with the ion excited states. The temperature-dependent study of the $^5D_J \rightarrow {}^7F_J$ transitions allowed to tentatively provide the Eu^{3+} intraionic assignments of the present diode structure. We have demonstrated that at least three non equivalent active sites are created by the Eu implantation in the diode structure: Eu1, Eu2 and Eu−Mg defect in its both configurations Eu0 and Eu1(Mg).

ASSOCIATED CONTENT

Supporting Information

The Supporting Information is available free of charge on the ACS Publications website at DOI: 10.1021/acsanm.8b00612.

Schematic diode structure and estimated Eu implanted penetration depth from the surface, 14 K PL excitation power dependence of the as-grown diode structure obtained with 325 nm laser excitation, PL temperature dependence of the as-grown diode structure obtained with 325 nm laser excitation, PLE fitting procedure, RT CEES spectra of the as-grown, HTHP, Eu14, and Eu15 samples, temperature dependence of $^5D_0 \rightarrow {}^7F_1$, and normalized high-resolution PL at 14 K and RT, around the $^5D_0 \rightarrow {}^7F_0$ region, for the Eu14 and Eu15 samples (PDF)

AUTHOR INFORMATION

Corresponding Author

*E-mail: nbensedrine@ua.pt.

ORCID

N. Ben Sedrine: 0000-0002-2255-3453

J. Rodrigues: 0000-0003-0424-3248

Notes

The authors declare no competing financial interest.

ACKNOWLEDGMENTS

The authors acknowledge financial support from FEDER funds through the POR Lisboa, COMPETE 2020 Programme and National Funds through FCT—Portuguese Foundation for Science and Technology under the projects UID/CTM/50025/2013, POCI-01-0145-FEDER-028011, and LISBOA-01-0145-FEDER-029666.

REFERENCES

(1) Wakahara, A.; Sekiguchi, H.; Okada, H.; Takagi, Y. Current Status for Light-Emitting Diode with Eu-Doped GaN Active Layer Grown by MBE. *J. Lumin.* **2012**, *132* (12), 3113−3117.

(2) O'Donnell, K.; Dierolf, V.. *Rare Earth Doped III-Nitrides for Optoelectronic and Spintronic Applications*; Springer, Canopus Academic Publishing Limited, 2010.

(3) *Rare Earth and Transition Metal Doping of Semiconductor Materials: Synthesis, Magnetic Properties and Room Temperature Spintronics*; Dierolf, V., Ferguson, I. T., Zavada, J. M., Eds.; Woodhead Publishing Series in Electronic and Optical Material 87; Elsevier, 2016.

(4) Nishikawa, A.; Furukawa, N.; Kawasaki, T.; Terai, Y.; Fujiwara, Y. Improved Luminescence Properties of Eu-Doped GaN Light-Emitting Diodes Grown by Atmospheric-Pressure Organometallic Vapor Phase Epitaxy. *Appl. Phys. Lett.* **2010**, *97* (5), 051113.

(5) Nishikawa, A.; Kawasaki, T.; Furukawa, N.; Terai, Y.; Fujiwara, Y. Room-Temperature Red Emission from a P-Type/europium-Doped/n-Type Gallium Nitride Light-Emitting Diode under Current Injection. *Appl. Phys. Express* **2009**, *2*, 071004.

(6) Bodiou, L.; Oussif, A.; Braud, A.; Doualan, J.-L.; Moncorgé, R.; Lorenz, K.; Alves, E. Effect of Annealing Temperature on Luminescence in Eu Implanted GaN. *Opt. Mater.* **2006**, *28*, 780−784.

(7) O'Donnell, K. P.; Roqan, I. S.; Wang, K.; Lorenz, K.; Alves, E.; Bockowski, M. The Photoluminescence/excitation (PL/E) Spectroscopy of Eu-Implanted GaN. *Opt. Mater.* **2011**, *33*, 1063−1065.

(8) Roqan, I. S.; O'Donnell, K. P.; Martin, R. W.; Edwards, P. R.; Song, S. F.; Vantomme, A.; Lorenz, K.; Alves, E.; Bockowski, M. Identification of the Prime Optical Center in GaN: Eu $^{3+}$. *Phys. Rev. B* **2010**, *81* (8), 85209.

(9) Mitchell, B.; Poplawsky, J.; Lee, D.; Koizumi, A.; Fujiwara, Y.; Dierolf, V. The Role of Donor-Acceptor Pairs in the Excitation of Eu-Ions in GaN: Eu Epitaxial Layers The Role of Donor-Acceptor Pairs in the Excitation of Eu-Ions in GaN: Eu Epitaxial Layers. *J. Appl. Phys.* **2014**, *115*, 204501.

(10) Mitchell, B.; Hernandez, N.; Lee, D.; Koizumi, A.; Fujiwara, Y.; Dierolf, V. Charge State of Vacancy Defects in Eu-Doped GaN. *Phys. Rev. B: Condens. Matter Mater. Phys.* **2017**, *96*, 64308.

(11) Kim, S.; Rhee, S. J.; Li, X.; Coleman, J. J.; Bishop, S. G. Selective Enhancement of 1540 nm Er^{3+} Emission Centers in Er-Implanted GaN by Mg Codoping. *Appl. Phys. Lett.* **2000**, *76* (17), 2403.

(12) Lee, D. G.; Nishikawa, A.; Terai, Y.; Fujiwara, Y. Eu Luminescence Center Created by Mg Codoping in Eu-Doped GaN. *Appl. Phys. Lett.* **2012**, *100*, 171904.

(13) O'Donnell, K. P.; Martin, R. W.; Edwards, P. R.; Lorenz, K.; Alves, E.; Bockowski, M. Temperature-Dependent Hysteresis of the Emission Spectrum of Eu-Implanted. *AIP Conf. Proc.* **2012**, *1566*, 63.

(14) O'Donnell, K. P.; Edwards, P. R.; Kappers, M. J.; Lorenz, K.; Alves, E.; Bockowski, M. Europium-Doped GaN(Mg): Beyond the Limits of the Light-Emitting Diode. *Phys. Status Solidi c* **2014**, *11*, 662.

(15) Singh, A. K.; O'Donnell, K. P.; Edwards, P. R.; Lorenz, K.; Kappers, M. J.; Bockowski, M. Hysteretic Photochromic Switching of Eu-Mg Defects in GaN Links the Shallow Transient and Deep Ground States of the Mg Acceptor. *Sci. Rep.* **2017**, *7*, 41982.

(16) Singh, A. K.; O'Donnell, K. P.; Edwards, P. R.; Cameron, D.; Lorenz, K.; Kappers, M. J.; Bockowski, M.; Yamaga, M.; Prakash, R. Luminescence of Eu $^{3+}$ in GaN (Mg, Eu): Transitions from the 5 D 1 Level. *Appl. Phys. Lett.* **2017**, *111*, 241105.

DOI: 10.1021/acsanm.8b00612
ACS Appl. Nano Mater. XXXX, XXX, XXX−XXX

(17) Ebdah, M. A.; Jadwisienczak, W. M.; Kordesch, M. E.; Ramadan, S.; Morkoç, H.; Anders, A. Studies of III-Nitride Superlattice Structures Implanted with Lanthanide Ions. *MRS Online Proc. Libr.* **2009**, *1111*, D04-12.
(18) Lozykowski, H. J.; Jadwisienczak, W. M.; Han, J.; Brown, I. G. Luminescence Properties of GaN and Al0.14Ga0.86N/GaN Superlattice Doped with Europium. *Appl. Phys. Lett.* **2000**, *77*, 767.
(19) Arai, T.; Timmerman, D.; Wakamatsu, R.; Lee, D. G.; Koizumi, A.; Fujiwara, Y. Enhanced Excitation Efficiency of Eu Ions in Eu-Doped GaN/AlGaN Multiple Quantum Well Structures Grown by Organometallic Vapor Phase Epitaxy. *J. Lumin.* **2015**, *158*, 70.
(20) Sobolev, N. A.; Emel'yanov, A. M.; Sakharov, V. I.; Serenkov, I. T.; Shek, E. I.; Besyul'kin, A. I.; Lundin, W. V.; Shmidt, N. M.; Usikov, A. S.; Zavarin, E. E. Photoluminescence in Er-Implanted AlGaN/GaN Superlattices and GaN Epilayers. *Phys. B* **2003**, *340*−*342*, 1108.
(21) Favennec, P. N.; L'Haridon, H.; Salvi, M.; Moutonnet, D.; Le Guillou, Y. Luminescence of Erbium Implanted in Various Semiconductors: IV, III-V and II-VI Materials. *Electron. Lett.* **1989**, *25* (11), 718.
(22) Wakahara, A. Impact of AlGaN on Luminescence Capability of Rare-Earth Ions in AlGaN. *Opt. Mater.* **2006**, *28*, 731.
(23) O'Donnell, K. P. The Temperature Dependence of the Luminescence of Rare-Earth-Doped Semiconductors: 25 Years after Favennec. *Phys. Status Solidi c* **2015**, *12* (4−5), 466.
(24) Kanemoto, M.; Sekiguchi, H.; Yamane, K.; Okada, H.; Wakahara, A. Eu^{3+} Luminescence Properties of Eu- and Mg-Codoped AlGaN. *J. Lumin.* **2015**, *166*, 60.
(25) Mishra, J. K.; Langer, T.; Rossow, U.; Shvarkov, S.; Wieck, A.; Hangleiter, A. Strong Enhancement of Eu^{+3} Luminescence in Europium-Implanted GaN by Si and Mg Codoping. *Appl. Phys. Lett.* **2013**, *102*, 061115.
(26) Lee, D.; Wakamatsu, R.; Koizumi, A.; Terai, Y.; Fujiwara, Y. Control of Eu Luminescence Centers by Codoping of Mg and Si into Eu-Doped GaN. *Jpn. J. Appl. Phys.* **2013**, *52*, 08JM01.
(27) Faye, D. N.; Fialho, M.; Magalhães, S.; Alves, E.; Ben Sedrine, N.; Rodrigues, J.; Correia, M. R.; Monteiro, T.; Boćkowski, M.; Hoffmann, V.; et al. Study of Damage Formation and Annealing of Implanted III-Nitride Semiconductors for Optoelectronic Devices. *Nucl. Instrum. Methods Phys. Res., Sect. B* **2016**, *379*, 251.
(28) Pipeleers, B.; Hogg, S. M.; Vantomme, A. Defect Accumulation during Channeled Erbium Implantation into GaN. *J. Appl. Phys.* **2005**, *98* (12), 123504.
(29) Lorenz, K.; Miranda, S. M. C.; Alves, E.; Roqan, I. S.; O'Donnell, K. P.; Bokowski, M. High Pressure Annealing of Europium Implanted GaN. *Proc. SPIE* **2012**, *8262*, 82620C.
(30) Mackova, A.; Malinský, P.; Sofer, Z.; Šimek, P.; Sedmidubský, D.; Mikulics, M.; Wilhelm, R. A. A Study of the Structural Properties of GaN Implanted by Various Rare-Earth Ions. *Nucl. Instrum. Methods Phys. Res., Sect. B* **2013**, *307*, 446.
(31) Kuball, M.; Hayes, J. M.; Suski, T.; Jun, J.; Leszczynski, M.; Domagala, J.; Tan, H. H.; Williams, J. S.; Jagadish, C. High-Pressure High-Temperature Annealing of Ion-Implanted GaN Films Monitored by Visible and Ultraviolet Micro-Raman Scattering. *J. Appl. Phys.* **2000**, *87* (6), 2736.
(32) Kuball, M.; Hayes, J. M.; Suski, T.; Jun, J.; Tan, H. H.; Williams, J. S.; Jagadish, C. The Use of Micro-Raman Spectroscopy to Monitor High-Pressure High- Temperature Annealing of Ion-Implanted GaN Films. *MRS Online Proc. Libr.* **1999**, *595*, F99W11.46.
(33) Holtz, M.; Zallen, R.; Brafman, O.; Matteson, S. Raman-Scattering Depth Profile of the Structure of Ion-Implanted GaAs. *Phys. Rev. B: Condens. Matter Mater. Phys.* **1988**, *37* (9), 4609.
(34) Kumar, M.; De Brabander, G. N.; Chen, P.; Boyd, J. T.; Steckl, A. J.; Choo, A. G.; Jackson, H. E.; Burnham, R. D.; Smith, S. C. Optical Channel Waveguides in AlGaAs Multiple Quantum Well Structures Formed by Focused Ion Beam Induced Compositional Mixing. *MRS Online Proc. Libr.* **1992**, *281*, 313−318.
(35) Christofides, C.; Ghibaudo, G. *Semiconductors and Semimetals Vol. 46: Effect of Disorder and Defects in Ion-Implanted Semiconductors: Optical and Photothermal Characterization*; Academic Press, 1997.
(36) Kuball, M. Raman Spectroscopy of GaN, AlGaN and AlN for Process and Growth Monitoring/control. *Surf. Interface Anal.* **2001**, *31* (10), 987−999.
(37) Puech, P.; Demangeot, F.; Frandon, J.; Pinquier, C.; Kuball, M.; Domnich, V.; Gogotsi, Y. GaN Nanoindentation: A Micro-Raman Spectroscopy Study of Local Strain Fields. *J. Appl. Phys.* **2004**, *96* (5), 2853.
(38) Correia, M. R.; Pereira, S.; Pereira, E.; Frandon, J.; Alves, E. Raman Study of the Phonon in Relaxed and Pseudomorphic InGaN Epilayers Raman Study of the A 1 (LO) Phonon in Relaxed and Pseudomorphic InGaN Epilayers. *Appl. Phys. Lett.* **2003**, *83* (23), 4761.
(39) Song, S. F.; Chen, W. D.; Zhang, C.; Bian, L.; Hsu, C. C.; Ma, B.; Li, G. H.; Zhu, J. Raman Scattering and Photoluminescence Studies of Er-Implanted and Er+O Coimplanted GaN. *J. Appl. Phys.* **2004**, *96* (9), 4930.
(40) Davydov, V. Y.; Kitaev, Y. E.; Goncharuk, I. N.; Smirnov, A. N.; Graul, J.; Semchinova, O.; Uffmann, D.; Smirnov, M. B.; Mirgorodsky, A. P.; Evarestov, R. A. Phonon Dispersion and Raman Scattering in Hexagonal GaN and AlN. *Phys. Rev. B: Condens. Matter Mater. Phys.* **1998**, *58* (19), 12899.
(41) Nipko, J. C.; Loong, C. K.; Balkas, C. M.; Davis, R. F. Phonon Density of States of Bulk Gallium Nitride Phonon Density of States of Bulk Gallium Nitride. *Appl. Phys. Lett.* **1998**, *73* (1), 34.
(42) Arguello, C. A.; Rousseau, D. L.; Porto, S. P. S. First-Order Raman Effect in Wurtzite-Type Crystals. *Phys. Rev.* **1969**, *181* (3), 1351.
(43) Demangeot, F.; Frandon, J.; Renucci, M. A.; Grandjean, N.; Beaumont, B.; Massies, J.; Gibart, P. Coupled Longitudinal Optic Phonon-Plasmon Modes in p-Type GaN. *Solid State Commun.* **1998**, *106* (8), 491.
(44) Harima, H. Properties of GaN and Related Compounds Studied by Means of Raman Scattering. *J. Phys.: Condens. Matter* **2002**, *14*, R967.
(45) Bulutay, C.; Dagli, N.; Imamoglu, A. Characterization of Excitons in Wurtzite GaN Quantum Wells under Valence Band. *IEEE J. Quantum Electron.* **1999**, *35* (4), 590.
(46) Kovalev, D.; Averboukh, B.; Volm, D.; Meyer, B. K.; Amano, H.; Akasaki, I. Free Exciton Emission in GaN. *Phys. Rev. B: Condens. Matter Mater. Phys.* **1996**, *54* (4), 2518.
(47) Alderighi, D.; Vinattieri, A.; Bogani, F.; Colocci, M.; Gottardo, S.; Grandjean, N.; Massies, J. Phonon Replica Dynamics in High Quality GaN Epilayers and AlGaN/GaN Quantum Wells. *Phys. status solidi a* **2001**, *183* (1), 129.
(48) Smith, M.; Lin, J. Y.; Jiang, H. X.; Salvador, A.; Botchkarev, A.; Kim, W.; Morkoc, H. Optical Transitions in $GaN/Al_xGa1_{-x}N$ Multiple Quantum Wells Grown by Molecular Beam Epitaxy. *Appl. Phys. Lett.* **1996**, *69*, 2453.
(49) Reshchikov, M. A.; Yi, G.-C.; Wessels, B. W. Behavior of 2.8- and 3.2-eV Photoluminescence Bands in Mg-Doped GaN at Different Temperatures and Excitation Densities. *Phys. Rev. B: Condens. Matter Mater. Phys.* **1999**, *59* (20), 13176.
(50) Alivov, Y. I.; Van Nostrand, J. E.; Look, D. C.; Chukichev, M. V.; Ataev, B. M. Observation of 430 nm Electroluminescence from ZnO/GaN Heterojunction Light-Emitting Diodes. *Appl. Phys. Lett.* **2003**, *83* (14), 2943.
(51) Nakamura, S.; Mukai, T.; Senoh, M. High-Power GaN p-n Junction Blue-Light-Emitting Diodes. *Jpn. J. Appl. Phys.* **1991**, *30*, L1998.
(52) Khan, M. A.; Chen, Q.; Skogman, R. A.; Kuznia, J. N. Violet-Blue GaN Homojunction Light Emitting Diodes with Rapid Thermal Annealed P-Type Layers. *Appl. Phys. Lett.* **1995**, *66* (16), 2046.
(53) Monemar, B.; Paskov, P.; Pozina, G.; Hemmingsson, C.; Bergman, J. P.; Khromov, S.; Izyumskaya, V. N.; Avrutin, V.; Li, X.; Morkoç, H.; et al. Properties of the Main Mg-Related Acceptors in

DOI: 10.1021/acsanm.8b00612
ACS Appl. Nano Mater. XXXX, XXX, XXX−XXX

GaN from Optical and Structural Studies. *J. Appl. Phys.* **2014**, *115*, 053507.
(54) Lany, S.; Zunger, A. Dual Nature of Acceptors in GaN and ZnO: The Curious Case of the Shallow Deep State. *Appl. Phys. Lett.* **2010**, *96*, 142114.
(55) Hautakangas, S.; Oila, J.; Alatalo, M.; Saarinen, K.; et al. Vacancy Defects as Compensating Centers in Mg-Doped GaN. *Phys. Rev. Lett.* **2003**, *90*, 137402.
(56) Reshchikov, M. A.; Morkoç, H. Luminescence Properties of Defects in GaN. *J. Appl. Phys.* **2005**, *97*, 061301.
(57) Nakarmi, M. L.; Nepal, N.; Lin, J. Y.; Jiang, H. X. Photoluminescence Studies of Impurity Transitions in Mg-Doped AlGaN Alloys. *Appl. Phys. Lett.* **2009**, *94*, 091903.
(58) Yan, Q.; Janotti, A.; Scheffler, M.; Van de Walle, C. G. Role of Nitrogen Vacancies in the Luminescence of Mg-Doped GaN. *Appl. Phys. Lett.* **2012**, *100* (14), 142110.
(59) Ben Sedrine, N.; Esteves, T. C.; Rodrigues, J.; Rino, L.; Correia, M. R.; Sequeira, M. C.; Neves, A. J.; Alves, E.; Bońkowski, M.; Edwards, P. R.; et al. Photoluminescence Studies of a Perceived White Light Emission from a Monolithic InGaN/GaN Quantum Well Structure. *Sci. Rep.* **2015**, *5*, 13739.
(60) Reshchikov, M. A.; McNamara, J. D.; Zhang, F.; Monavarian, M.; Usikov, A.; Helava, H.; Makarov, Y.; Morkoç, H. Zero-Phonon Line and Fine Structure of the Yellow Luminescence Band in GaN. *Phys. Rev. B: Condens. Matter Mater. Phys.* **2016**, *94*, 35201.
(61) Lyons, J. L.; Janotti, A.; Van De Walle, C. G. Carbon Impurities and the Yellow Luminescence in GaN. *Appl. Phys. Lett.* **2010**, *97*, 152108.
(62) Christenson, S. G.; Xie, W.; Sun, Y. Y.; Zhang, S. B. Carbon as a Source for Yellow Luminescence in GaN: Isolated CN Defect or its Complexes. *J. Appl. Phys.* **2015**, *118*, 135708.
(63) Demchenko, D. O.; Diallo, I. C.; Reshchikov, M. A. Yellow Luminescence of Gallium Nitride Generated by Carbon Defect Complexes. *Phys. Rev. Lett.* **2013**, *110*, 87404.
(64) Reshchikov, M. A.; Demchenko, D. O.; Usikov, A.; Helava, H.; Makarov, Y. Carbon Defects as Sources of the Green and Yellow Luminescence Bands in Undoped GaN. *Phys. Rev. B: Condens. Matter Mater. Phys.* **2014**, *90*, 235203.
(65) Reshchikov, M. A.; Demchenko, D. O.; Mcnamara, J. D.; Fernandez-Garrido, S.; Calarco, R. Green Luminescence in Mg-Doped GaN. *Phys. Rev. B: Condens. Matter Mater. Phys.* **2014**, *90*, 35207.
(66) Contreras, S.; Konczewicz, L.; Peyre, H.; Juillaguet, S.; Al Khalfaoui, M.; Matta, S.; Leroux, M.; Damilano, B.; Brault, J. High Temperature Annealing of MBE-Grown Mg- Doped GaN. *J. Phys.: Conf. Ser.* **2017**, *864*, 012018.
(67) Nakamura, S.; Mukai, T.; Senoh, M.; Iwasa, N. Thermal Annealing Effects on p-Type Mg-Doped GaN Films. *Jpn. J. Appl. Phys.* **1992**, *31*, L139.
(68) Bell, A.; Liu, R.; Ponce, F. A.; Amano, H.; Akasaki, I.; Cherns, D. Light Emission and Microstructure of Mg-Doped AlGaN Grown on Patterned Sapphire. *Appl. Phys. Lett.* **2003**, *82*, 349.
(69) Li, J.; Oder, T. N.; Nakarmi, M. L.; Lin, J. Y.; Jiang, H. X. Optical and Electrical Properties of Mg-Doped P-Type AlxGa1-xN. *Appl. Phys. Lett.* **2002**, *80*, 1210.
(70) Ben Sedrine, N.; Rodrigues, J.; Cardoso, J.; Faye, D. N.; Fialho, M.; Magalhães, S.; Martins, A. F.; Neves, A. J.; Alves, E.; Bockowski, M.; et al. Optical Investigations of Europium Ion Implanted in Nitride-Based Diode Structures. *Surf. Coat. Technol.* **2018**, DOI: 10.1016/j.surfcoat.2018.02.004.
(71) Friel, I.; Thomidis, C.; Fedyunin, Y.; Moustakas, T. D. Investigation of Excitons in AlGaN/GaN Multiple Quantum Wells by Lateral Photocurrent and Photoluminescence Spectroscopies. *J. Appl. Phys.* **2004**, *95*, 3495.
(72) Martin, R. W.; Middleton, P. G.; O'Donnell, K. P.; Van Der Stricht, W. Exciton Localization and the Stokes' Shift in InGaN Epilayers. *Appl. Phys. Lett.* **1999**, *74*, 263.
(73) Kumagai, M.; Nishida, T.; Ando, H.; Kobayashi, N. Absorption Properties of the GaN/AlGaN Multiple Quantum Wells Grown on SiC Substrate. *IEEE* **1999**, 953.
(74) Badcock, T. J.; Dawson, P.; Kappers, M. J.; McAleese, C.; Hollander, J. L.; Johnston, C. F.; Rao, D. V. S.; Sanchez, A. M.; Humphreys, C. J. Optical Properties of GaN/AlGaN Quantum Wells Grown on Nonpolar Substrates. *Appl. Phys. Lett.* **2008**, *93*, 101901.
(75) Nyein, E. E.; Hömmerich, U.; Heikenfeld, J.; Lee, D. S.; Steckl, A. J.; Zavada, J. M. Spectral and Time-Resolved Photoluminescence Studies of Eu-Doped GaN. *Appl. Phys. Lett.* **2003**, *82*, 1655.
(76) Wang, K.; Martin, R. W.; O'Donnell, K. P.; Katchkanov, V.; Nogales, E.; Lorenz, K.; Alves, E.; Ruffenach, S.; Briot, O. Selectively Excited Photoluminescence from Eu-Implanted GaN. *Appl. Phys. Lett.* **2005**, *87*, 112107.
(77) Hughes, P. J.; Weiss, B. L.; Jackson, H. E. Composition and Confinement Energies of Interdiffused AlGaAs/GaAs Single Quantum Well Structures. *Semicond. Sci. Technol.* **1997**, *12*, 808.
(78) Binnemans, K. Interpretation of europium(III) Spectra. *Coord. Chem. Rev.* **2015**, *295*, 1−45.
(79) Gruber, J. B.; Vetter, U.; Taniguchi, T.; Burdick, G. W.; Hofsäss, H.; Chandra, S.; Sardar, D. K. Spectroscopic Analysis of Eu^{3+} in Single-Crystal Hexagonal Phase AlN. *J. Appl. Phys.* **2011**, *110*, 023104.
(80) Fleischman, Z.; Munasinghe, C.; Steckl, A. J.; Wakahara, A.; Zavada, J.; Dierolf, V. Excitation Pathways and Efficiency of Eu Ions in GaN by Site-Selective Spectroscopy. *Appl. Phys. B: Lasers Opt.* **2009**, *97*, 607.
(81) Rodrigues, J.; Leitão, M. F.; Carreira, J. F. C.; Ben Sedrine, N.; Santos, N. F.; Felizardo, M.; Auzelle, T.; Daudin, B.; Alves, E.; Neves, A. J.; et al. Spectroscopic Analysis of Eu^{3+} Implanted and Annealed GaN Layers and Nanowires. *J. Phys. Chem. C* **2015**, *119*, 17954.
(82) Peng, H.; Lee, C. W.; Everitt, H. O.; Munasinghe, C.; Lee, D. S.; Steckl, A. J. Spectroscopic and Energy Transfer Studies of Eu^{3+} Centers in GaN. *J. Appl. Phys.* **2007**, *102*, 073520.
(83) Woodward, N.; Nishikawa, A.; Fujiwara, Y.; Dierolf, V. Site and Sample Dependent Electron-Phonon Coupling of Eu Ions in Epitaxial-Grown GaN Layers. *Opt. Mater.* **2011**, *33*, 1050.
(84) Son, C. S.; Kim, S. I.; Kim, Y. H.; Kim, Y. T.; Choi, I. H.; Wakahara, A.; Tanoue, H.; Ogura, M. Red Emission from Eu-Implanted GaN. *J. Korean Phys. Soc.* **2004**, *45*, S519−S521.
(85) Rodrigues, J.; Leitão, M. F.; Carreira, J. F. C.; Ben Sedrine, N.; Santos, N. F.; Felizardo, M.; Auzelle, T.; Daudin, B.; Alves, E.; Neves, A. J.; et al. Correction to " Spectroscopic Analysis of Eu^{3+} Implanted and Annealed GaN Layers and Nanowires. *J. Phys. Chem. C* **2016**, *120*, 6907.
(86) Koizumi, A.; Kawabata, K.; Lee, D.; Nishikawa, A.; Terai, Y.; Ofuchi, H.; Honma, T.; Fujiwara, Y. In Situ Eu Doping into $Al_xGa_{1-x}N$ Grown by Organometallic Vapor Phase Epitaxy to Improve Luminescence Properties. *Opt. Mater.* **2015**, *41*, 75.
(87) Wang, K.; O'Donnell, K. P.; Hourahine, B.; Martin, R. W.; Watson, I. M.; Lorenz, K.; Alves, E. Luminescence of Eu Ions in Al_xGa_{1-X} N across the Entire Alloy Composition Range. *Phys. Rev. B: Condens. Matter Mater. Phys.* **2009**, *80*, 125206.
(88) O'Donnell, K. P.; Edwards, P. R.; Yamaga, M.; Lorenz, K.; Kappers, M. J.; Bońkowski, M. Crystal field Symmetries of Luminescent Eu^{3+} Centers in GaN: The Importance of the 5D0 to 7F1 Transition. *Appl. Phys. Lett.* **2016**, *108*, 022102.
(89) Monteiro, T.; Boemare, C.; Soares, M. J.; Sa Ferreira, R. A.; Carlos, L. D.; Lorenz, K.; Vianden, R.; Alves, E. Photoluminescence and Lattice Location of Eu and Pr Implanted GaN Samples. *Phys. B* **2001**, *308−310*, 22−25.
(90) O'Donnell, K. P.; Katchkanov, V.; Wang, K.; Martin, R. W.; Edwards, P. R.; Hourahine, B.; Nogales, E.; Mosselmans, J. F. W.; De Vries, B. Site Multiplicity of Rare Earth Ions in III-Nitrides. *MRS Online Proc. Libr.* **2004**, *831*, E9.6.
(91) Katchkanov, V.; O'Donnell, K. P.; Dalmasso, S.; Martin, R. W.; Braud, A.; Nakanishi, Y.; Wakahara, A.; Yoshida, A. Photoluminescence Studies of Eu-Implanted GaN Epilayers. *Phys. Status Solidi B* **2005**, *242*, 1491.

DOI: 10.1021/acsanm.8b00612
ACS Appl. Nano Mater. XXXX, XXX, XXX−XXX

Supporting Information

Eu-doped AlGaN/GaN superlattice-based diode structure for red lighting: Excitation mechanisms and active sites

N. Ben Sedrine[1,*], J. Rodrigues[1], D. Nd. Faye[2], A. J. Neves[1], E. Alves[2], M. Bockowski[3], V. Hoffmann[4], M. Weyers[4], K. Lorenz[2,5], M. R. Correia[1], and T. Monteiro[1]

[1]Departamento de Física e I3N, Universidade de Aveiro, Campus Universitário de Santiago, 3810-193 Aveiro, Portugal

[2]IPFN, Instituto Superior Técnico, Campus Tecnológico e Nuclear, Estrada Nacional 10, P-2695-066 Bobadela LRS, Portugal

[3]Institute of High Pressure Physics, Polish Academy of Sciences, 01-142 Warsaw, Poland

[4]Ferdinand-Braun-Institut, Leibniz-Institut für Höchstfrequenztechnik, Gustav-Kirchhoff-Straße 4, 12489 Berlin, Germany

[5]Instituto de Engenharia de Sistemas de Computadores - Microsystems and Nanotechnology (INESC-MN), Rua Alves Redol, 1000-029 Lisboa, Portugal

[*]Correspondence to nbensedrine@ua.pt

*** Schematic diode structure**

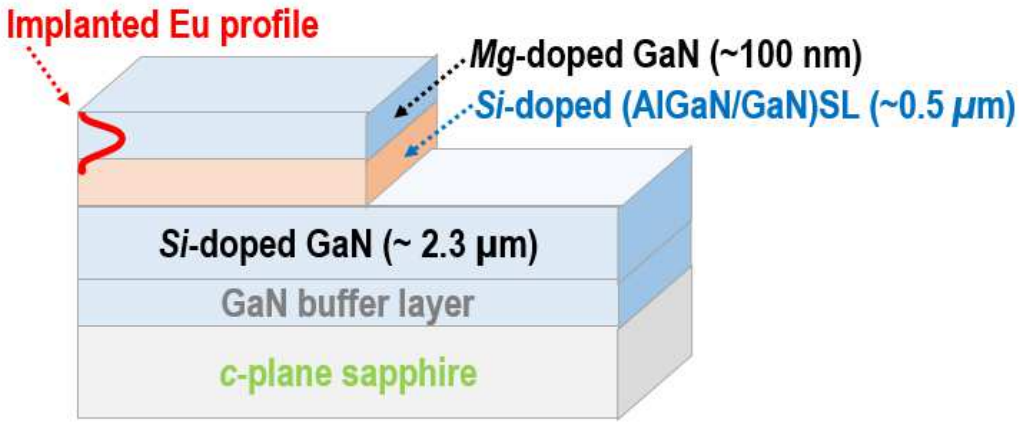

Figure S1: Schematic diode structure and estimated Eu implanted penetration depth from the surface (red curve).

*** Temperature and excitation power PL dependences of as-grown diode structure:**

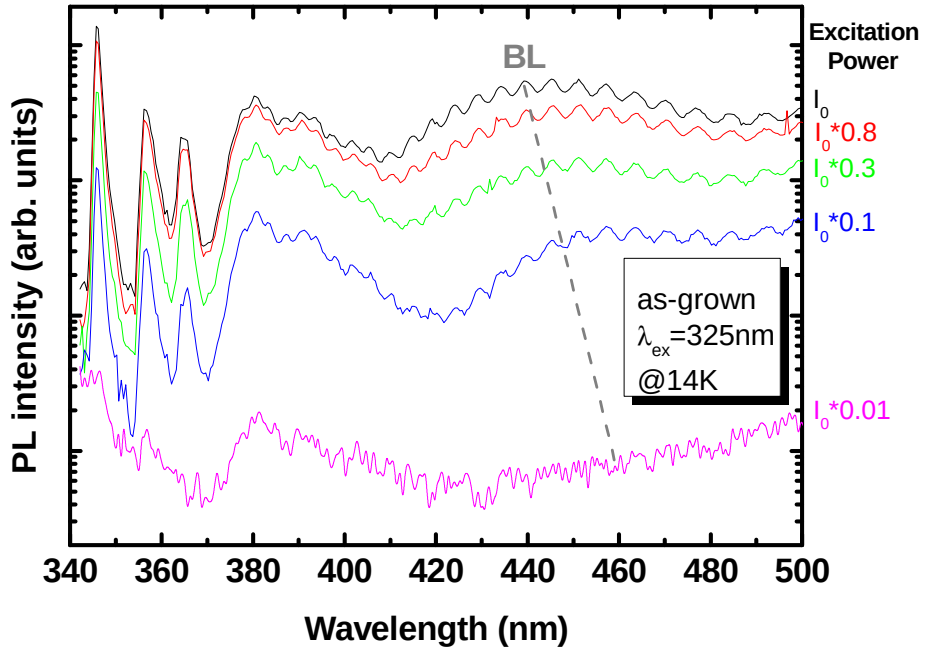

Figure S2: 14 K PL excitation power dependence of the as-grown diode structure obtained with 325 nm laser excitation.

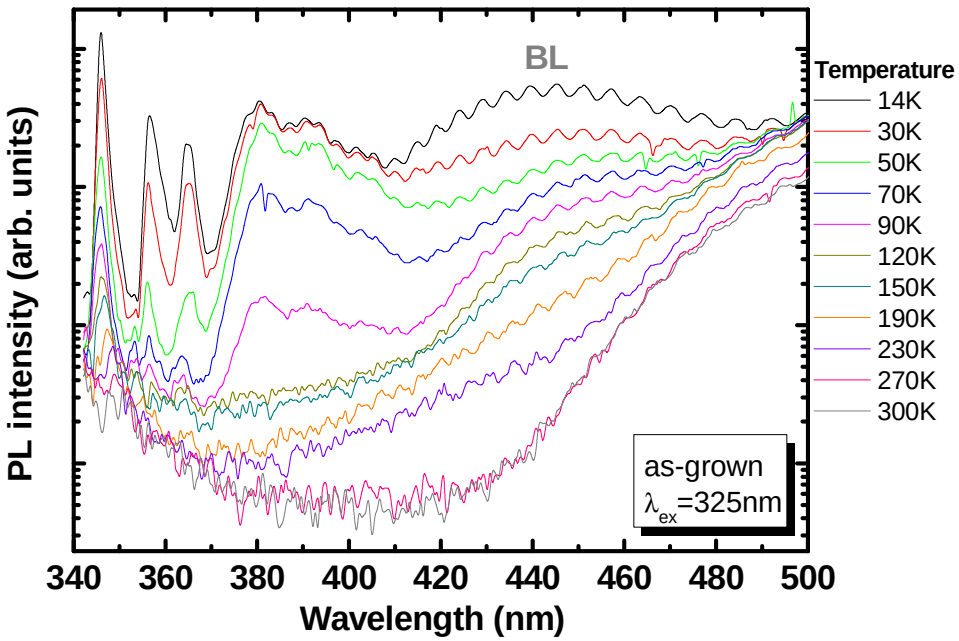

Figure S3: PL temperature dependence of the as-grown diode structure obtained with 325 nm laser excitation.

*** PLE fitting procedure:**

The PLE spectra of the as-grown sample were first fitted using eq. 1, and then the obtained best-fit parameters were used as input initial values for the rest of the samples. Due to the high number of parameters, we first assumed that no change of the energy positions occurred after Eu implantation and HTHP annealing with respect to the as-grown sample. In particular, the effective bandgap ϵ_s was kept constant for all the samples. In order to improve the quality of the fit, the energy positions were allowed to vary in a second step of the fitting procedure. Unlike the Lorentzian function, the Gaussian function corresponding to an inhomogeneous broadening is found to best describe the different transitions in our PLE experimental data. In Fig. 4 (f), the energy values used in the fitting procedure are similar to the ones used for the other samples, but a higher ϵ_3 energy value was needed to better describe the PLE of the Eu15 sample.

*** Combined excitation emission spectra (CEES):**

CEES spectra of the as-grown, HTHP, Eu14 and Eu15 samples were acquired at RT under the same experimental conditions and represented for the same intensity scale (Figure S4). CEE spectroscopy consists of measuring the emission spectrum for each excitation wavelength (from 320 to 420 nm). Noticeable changes could be observed in Figure S4: for the as-grown sample, the YL can be observed by pumping in the wavelength range 320-370 nm, while after HTHP annealing, the same emission can be observed by pumping in a broader wavelength range: 320-380 nm. After Eu implantation/HTHP annealing, the YL can be observed by pumping using a narrower wavelength range which is decreasing by increasing the Eu fluence; from 340 to 380 nm for the Eu14 sample, and from 345 to 375 nm for the Eu15 sample. Regarding the Eu-related sharp luminescence lines observed in the red spectral region at ~621 nm, they can be identified by pumping both samples with above and below GaN bandgap excitation energy. It is interesting to notice that the Eu^{3+} emission can be selectively pumped by using below GaN bandgap excitation energies through the broad excitation band tail (seen in Fig. 4 (f)).

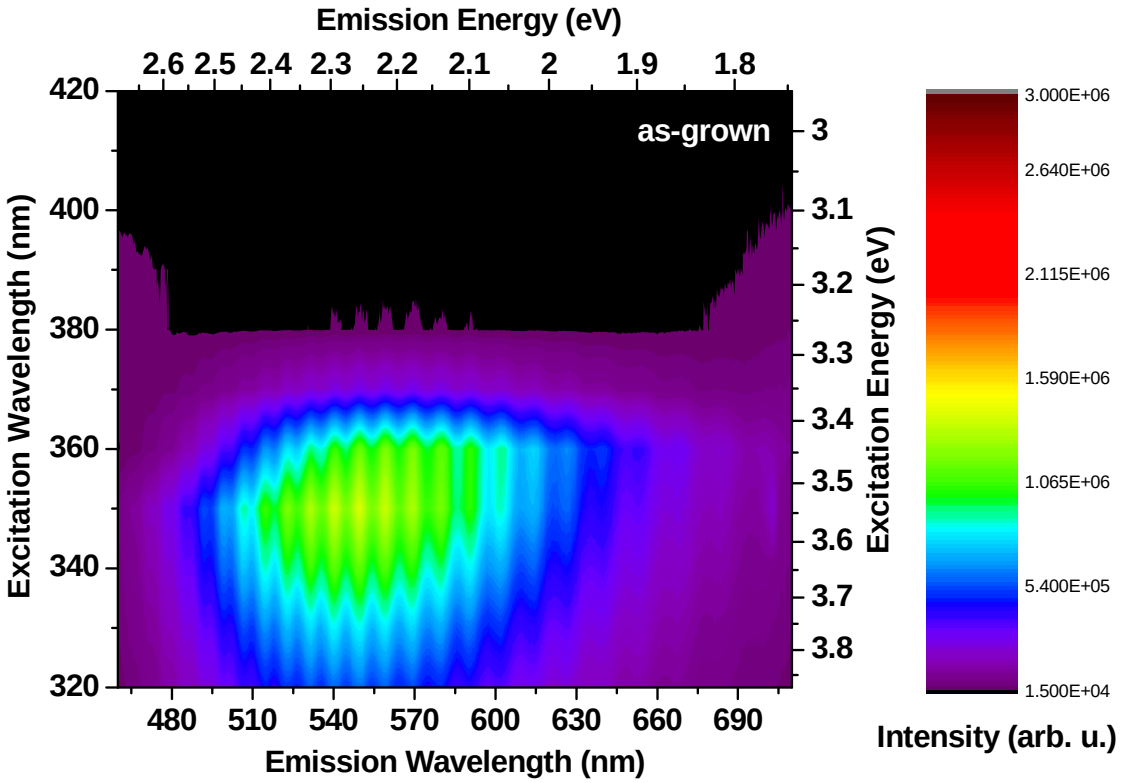
Emission Energy (eV)
2.6 2.5 2.4 2.3 2.2 2.1 2 1.9 1.8
as-grown
Excitation Wavelength (nm)
420 400 380 360 340 320
Excitation Energy (eV)
3 3.1 3.2 3.3 3.4 3.5 3.6 3.7 3.8
480 510 540 570 600 630 660 690
Emission Wavelength (nm)
3.000E+06
2.640E+06
2.115E+06
1.590E+06
1.065E+06
5.400E+05
1.500E+04
Intensity (arb. u.)

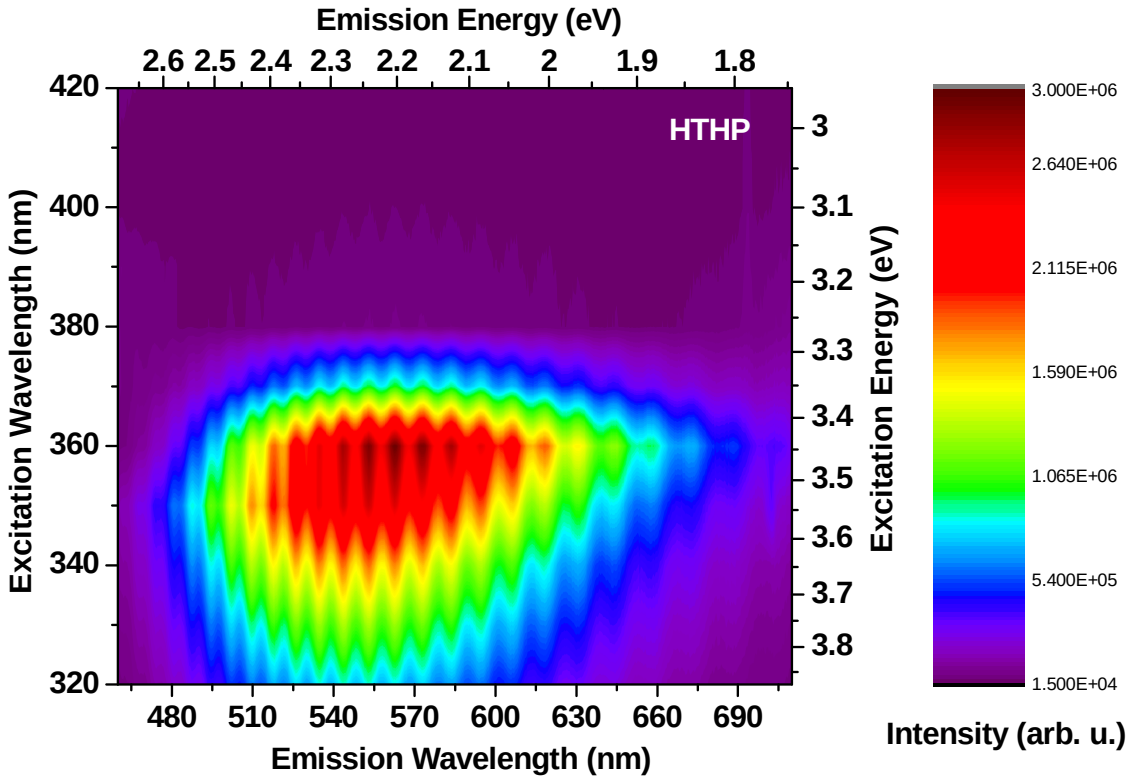
Emission Energy (eV)
2.6 2.5 2.4 2.3 2.2 2.1 2 1.9 1.8
HTHP
Excitation Wavelength (nm)
420 400 380 360 340 320
Excitation Energy (eV)
3 3.1 3.2 3.3 3.4 3.5 3.6 3.7 3.8
480 510 540 570 600 630 660 690
Emission Wavelength (nm)
3.000E+06
2.640E+06
2.115E+06
1.590E+06
1.065E+06
5.400E+05
1.500E+04
Intensity (arb. u.)

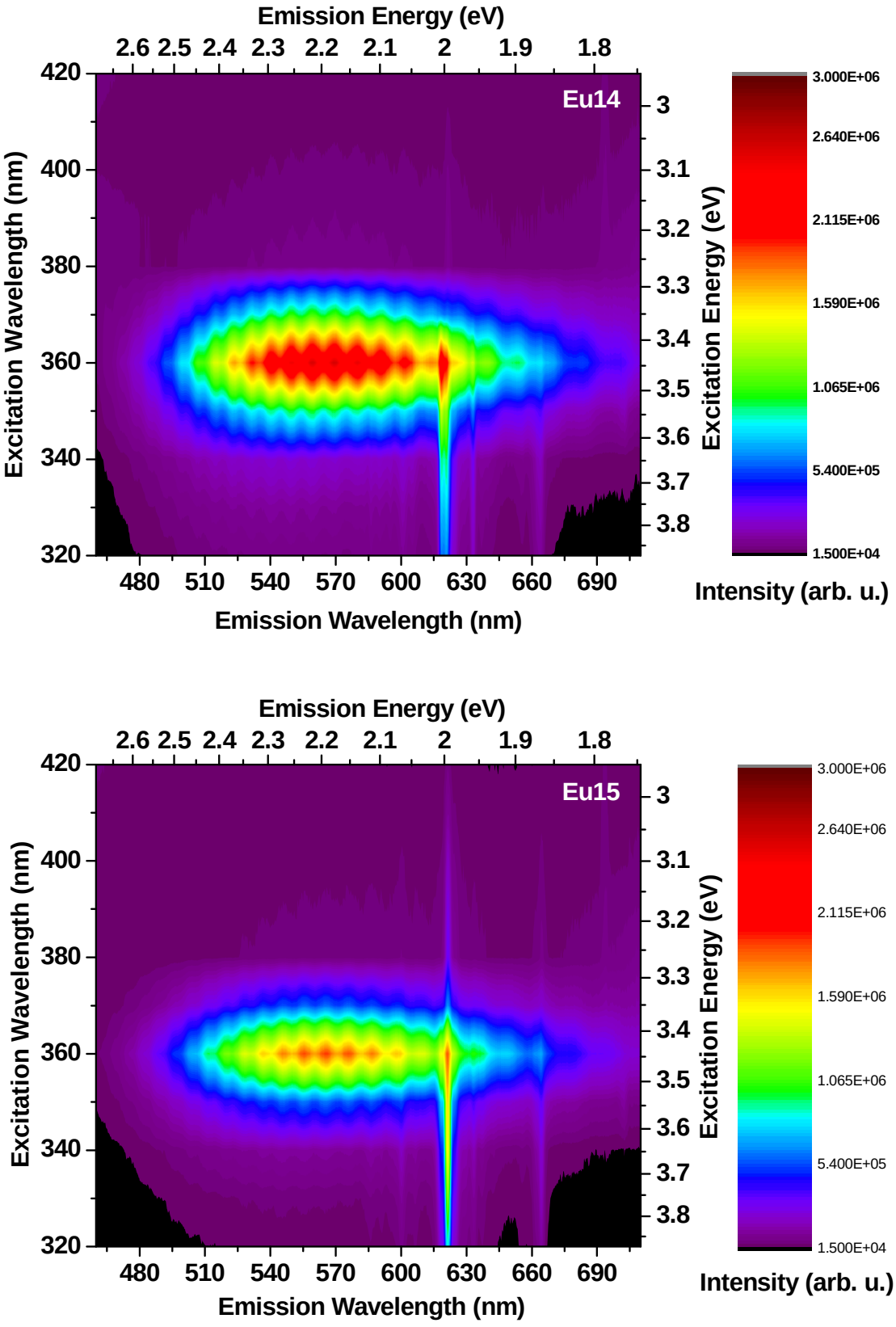

Figure S4: RT CEES spectra of the as-grown, HTHP, Eu14 and Eu15 samples.

*** Temperature dependence of $^5D_0 \rightarrow {}^7F_1$**

We have followed a similar procedure as the one used by Peng *et al.*[1] based on the fact that the spacing of the ^5D_J and ^7F_J levels remains the same from site to site and that only the $^5D_J \rightarrow {}^7F_J$ transitions exhibit a measurable, constant, site-dependent energy shift ΔE with respect to the highest energy transition (Q1). Such procedure was confirmed by the same authors using time-resolved PL[1]. The obtained energy spacing is of 5 and 7 meV for the Q2 and Q3 transitions, respectively, as indicated in Fig. 5 (c) and Table 2. The site-dependent energy shifts ΔE in R4, R5 and R6 transitions were found to be: 4.2 and 7 meV, respectively, with respect to the R_4 transition. In addition, the temperature dependence of these peaks clearly follows a similar behavior as the one of Q1, Q2 and Q3 transitions. Therefore, it is possible to correlate the sites involved in the R4, R5 and R6 transitions to the same ones involved in the Q1, Q2 and Q3 transitions, respectively. Since the R1, R2 and R3 peaks are broader and could be influenced by *J*-mixing, as reported for $^5D_0 \rightarrow {}^7F_1$ transition by K. Binnemans[2], a similar approach is less straightforward. Indeed, the sites R2 and R3 correspond to the Eu0 and Eu1(Mg) defect configurations obtained by O'Donnell *et al.* [3,4] in Eu-implanted and annealed Mg-doped GaN layers, corresponding to near-axial sites [3,4].

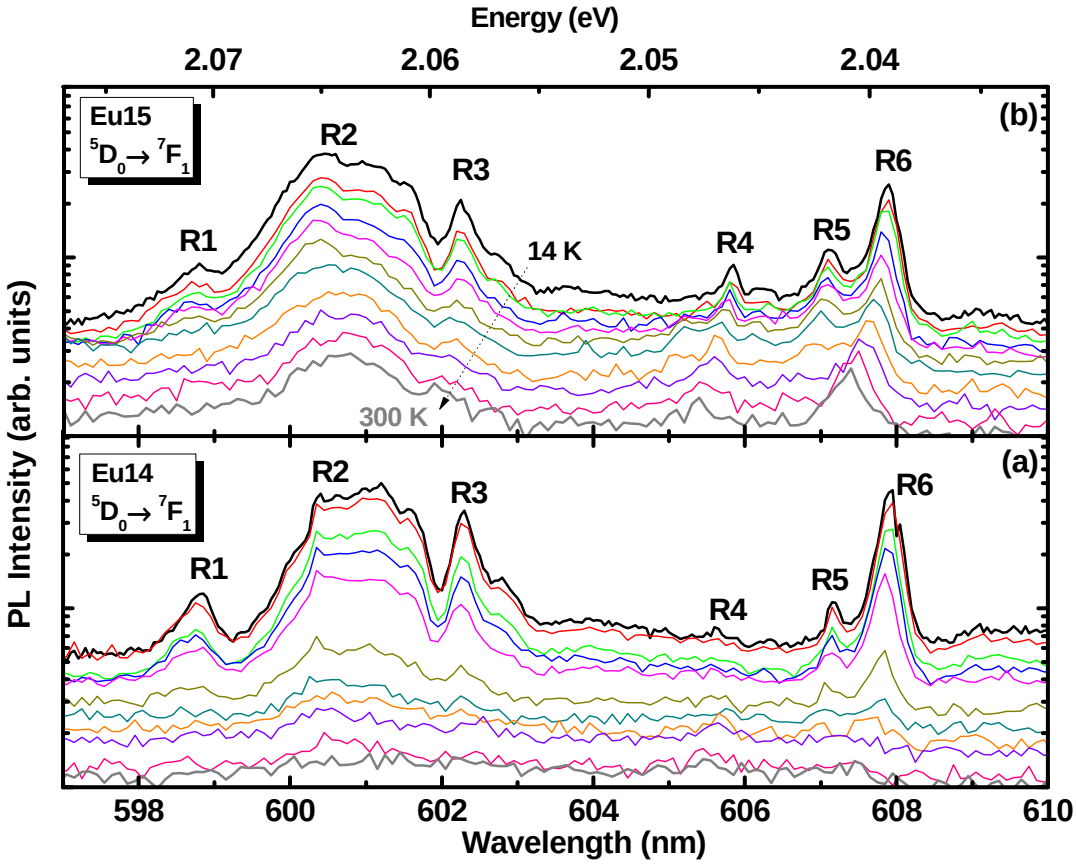

Figure S5: High-resolution temperature dependence PL for the Eu14 (a) and Eu15 (b) samples around the $^5D_0 \rightarrow {}^7F_1$ region.

*** Comparison of Eu14 and Eu15 samples around the $^5D_0 \rightarrow {}^7F_0$ transition:**

A comparison of the normalized PL intensity, around the $^5D_0 \rightarrow {}^7F_0$ transition, is analyzed for both Eu implanted and annealed samples, at RT (a) and 14 K (b) (Figure S6). It is known that for continuous wave excitation, the relative strength of the main peaks may be taken as a rough indication of the relative concentration of Eu^{3+} dopants at each site[1]. According to Fleischman *et al.* [5] and O'Donnell *et al.* [6], above bandgap excitation renders a dominant emission from the main site, and the minority sites MS 3, 4, and 5 (related to deep defect traps), but also contributions from other minority sites (related to shallow traps) can be seen. We found that for such above bandgap excitation, the Q1 site has a significantly higher excitation efficiency compared to the Q2 site for Eu15 sample, both at low and room temperature.

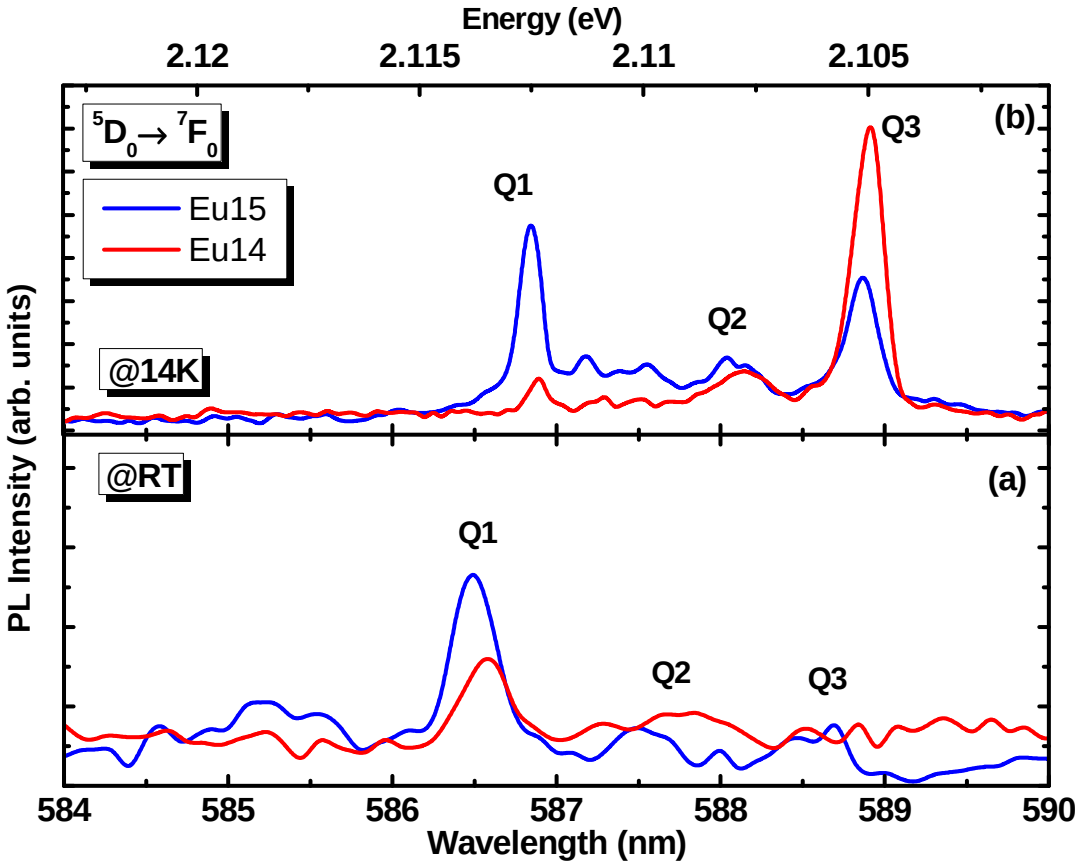

Figure S6: Normalized high-resolution PL at 14 K (a) and at RT (b), around the $^5D_0 \rightarrow {}^7F_0$ region, for the Eu14 and Eu15 samples.

REFERENCES

(1) Peng, H.; Lee, C. W.; Everitt, H. O.; Munasinghe, C.; Lee, D. S.; Steckl, A. J. Spectroscopic and Energy Transfer Studies of Eu^{3+} Centers in GaN. *J. Appl. Phys.* **2007**, *102*, 73520.

(2) Binnemans, K. Interpretation of europium(III) Spectra. *Coord. Chem. Rev.* **2015**, *295*, 1–45.

(3) Singh, A. K.; O'Donnell, K. P.; Edwards, P. R.; Cameron, D.; Lorenz, K.; Kappers, M. J.; Boćkowski, M.; Yamaga, M.; Prakash, R. Luminescence of Eu 3 1 in GaN (Mg , Eu): Transitions from the 5 D 1 Level. *Appl. Phys. Lett.* **2017**, *111*, 241105.

(4) O'Donnell, K. P.; Edwards, P. R.; Yamaga, M.; Lorenz, K.; Kappers, M. J.; Boćkowski, M. Crystal field Symmetries of Luminescent Eu^{3+} Centers in GaN: The Importance of the 5D0 to 7F1 Transition. *Appl. Phys. Lett.* **2016**, *108*, 22102.

(5) Fleischman, Z.; Munasinghe, C.; Steckl, A. J.; Wakahara, A.; Zavada, J.; Dierolf, V. Excitation Pathways and Efficiency of Eu Ions in GaN by Site-Selective Spectroscopy. *Appl. Phys. B* **2009**, *97*, 607.

(6) O'Donnell, K. P.; Katchkanov, V.; Wang, K.; Martin, R. W.; Edwards, P. R.; Hourahine, B.; Nogales, E.; Mosselmans, J. F. W.; De Vries, B.; Consortium, Ren. Site Multiplicity of Rare Earth Ions in III-Nitrides. *Mater. Res. Soc. Symp. Proc.* **2005**, *831*, E9.6.